

# Controls on the Deformation of the Central and Southern Andes (10–35° S): Insight from Thin-Sheet Numerical Modeling

Sergei Medvedev · Yuri Podladchikov · Mark R. Handy · Ekkehard Scheuber

**Abstract.** What mechanisms and conditions formed the Central Andean orocline and the neighboring Altiplano Plateau? Why does deformation decrease going from the central to the Southern Andes? To answer these questions, we present a new thin-sheet model that incorporates three key features of subduction orogenesis: (1) significant temporal and spatial changes in the strength of the continental lithosphere in the upper plate; (2) variable interplate coupling along a weak subduction channel with effectively anisotropic mechanical properties; and (3) channeled flow of partially molten lower crust in the thickened upper plate. Application of this model to the present kinematic situation between the Nazca and South American Plates indicates that the deformed Andean lithosphere is significantly weaker than the undeformed South American foreland, and that channel flow of partially melted lower crust smoothes topographic relief. This channel flow is, therefore, inferred to control intra-orogenic topography and is primarily responsible for the development of the Andean Plateau since the Miocene. A parameter study shows that the decrease in shortening rates from the central to the Southern Andes can be attributed to the weakening of the orogenic Andean lithosphere and to along-strike variations in interplate coupling within the subduction zone. The current rates of deformation are reproduced in the model if: the Andean lithosphere is assumed to be 5–15 times weaker than the lithosphere of the Brazilian shield; interplate coupling is assumed to be relatively weak, such that the subduction zone in the vicinity of the Central Andes is some 10–20 times weaker than the Andean lithosphere; and coupling itself decreases laterally by some 2–5 times going from the central to the Southern Andes.

## 23.1 Introduction

The bend of the Andes, known as the Bolivian orocline (Fig. 23.1), is a first-order structure visible from space. Oroclinal bending in the Andes was originally proposed by Carey (1958) to have involved anticlockwise rotation of the Andes north of the Arica bend (Fig. 23.1) superposed on an initially straight Andean chain. Indeed, paleomagnetic studies have revealed a consistent and roughly symmetrical pattern of anticlockwise rotations north of the Arica bend and of clockwise rotations south of it (e.g., MacFadden et al. 1995). Today, however, there is consensus that the Central Andes were never entirely straight (Sheffels 1995) and that the original curvature of the plate margin was enhanced during Andean orogenesis rather than having been imposed later (Isacks 1988).

Here, we refer to the segment of the Central Andes containing the Andean Plateau as the Central Andes (lower case in “central”), reaching from ~16° S to 25° S. Parts of Andes south of this latitude to the southern limit of our model we term the Southern Andes. Our subdivision differs from the traditional division of the Andean chain into Central and Southern Andes at ~30° S (Gansser 1973), and reflects the north-to-south change in morphology and rates of deformation, as discussed throughout this paper.

Several explanations have been given for the development of the Bolivian orocline. Isacks (1988) and Allmendinger et al. (1997) argued that the bending resulted from

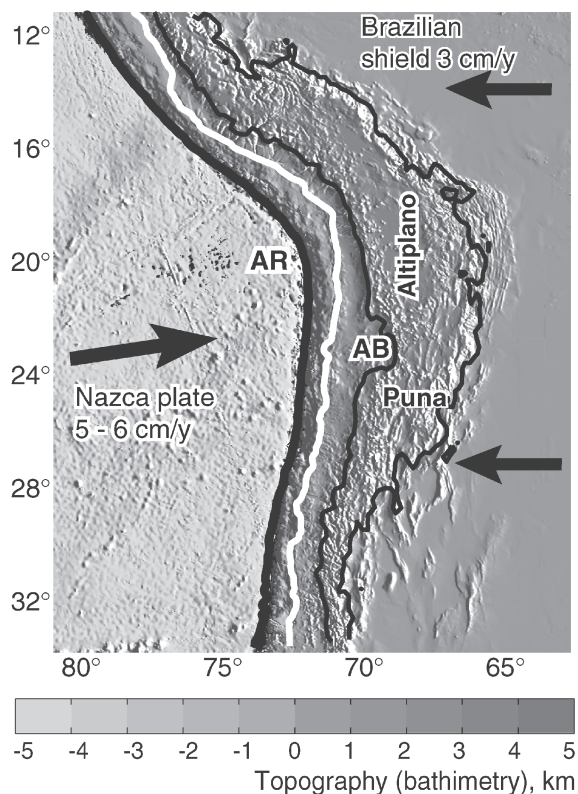


**Fig. 23.1.** Topography and bathymetry of the adjoining Nazca and South American Plates. Plate boundary (thick black line), coastal line (white line), 3 km elevation line (thin black line), Atacama Basin (AB), Altiplano and Puna Plateaus, Arica bend (AR)

differential shortening along the Andean chain, with shortening increasing towards the Arica bend. Kley et al. (1999) have shown how oroclinal bending could have been achieved by differential shortening. In their model, several fault-bounded blocks underwent various degrees of displacement and differential rotation. Shortening estimates require that rotation of the limbs of the orocline did not exceed 5–10°. Riller and Oncken (2003) also related oroclinal bending to orogen-parallel gradients in horizontal shortening plus block rotations and strike-slip movements. These authors linked these movements to the orogen-normal growth of the Central Andean Plateaus.

Numerical models of Liu et al. (2002) and Yang et al. (2003) set boundary conditions at the western margin of the South America that effectively prescribe the evolution of this margin and preclude modeling the bending of the orocline. Yanez and Cembrano (2004) used a thin sheet approximation model to show that along-strike variations in coupling between Nazca and South American Plates can result in bending of the western boundary of the Central Andes. Sobolev et al. (Chap. 25 of this volume) uses a model that incorporates laws of empirical flow and a coupled thermomechanical approach to compare the evolution of the central and Southern Andes, yet the application of their two-dimensional (2D) modeling to the problem of oroclinal bending, effectively a three-dimensional (3D) process, should be tested using a 3D approach sometime in future. Here, we present a complementary approach to that of Sobolev et al. (2006, Chap. 25 of this volume) by considering a map view of deformational processes in the Andes.

As noted above, the Bolivian orocline is spatially related to another primary structure, the Central Andean Altiplano-Puna Plateau, which, following the Tibetan Plateau, is the second largest plateau on Earth (Fig. 23.1). The thick crust underlying the plateau (> 70 km, James 1971; Wigger et al. 1994; Zandt et al. 1994; Giese et al. 1999; Yuan et al. 2000) is mainly attributed to crustal shortening (Isacks 1988). There are differences between the Altiplano and Puna parts of the plateau: The Puna is slightly higher and has greater relief than the Altiplano. Moreover, the lithosphere is thicker beneath the central and eastern parts of the Altiplano (70–80 km), but less thick (60–70 km) beneath the westernmost Altiplano and Puna (Whitman et al. 1992).

In a synthesis of space-geodetic measurements, Neogene shortening data, and paleomagnetic data, Lamb (2000) has shown that the Altiplano is currently growing eastwards (see also Oncken et al., Chap. 1 of this volume; Sobolev et al., Chap. 25 of this volume) without significant uplift of the plateau (in contrast to the results of Yang et al. 2003). Numerical models of orogenesis that incorporate plateau evolution attribute the relatively low relief in the central part of the Himalayan and Andean chains to the lateral flow of weak, possibly partially molten, rock

in a middle to lower crustal channel within the thickened orogenic crust (Beaumont et al. 2001, 2004; Vanderhaeghe et al. 2003; Royden 1996; Shen et al. 2001).

Channel flow is driven by differential pressure associated with topographic gradients, such that highly mobile, viscous crust flows from beneath areas of greater to lesser elevation. In flattening topographic gradients, channel flow can form orogenic plateaus as shown in a number of numerical experiments (e.g., Shen et al. 2001; Husson and Sempere 2003; Medvedev and Beaumont, in press). Thermal conditions beneath the Altiplano Plateau favor partial melting (Springer 1999; Springer and Förster 1998; Brasse et al. 2002; Babeyko et al. 2002) and therefore makes channel flow a viable mechanism for the formation of the Andean Plateaus, as already proposed by Husson and Sempere (2003) and Gerbault et al. (2005).

The change in style and in the amount of deformation along the Andean orogenic belt also requires explanation. Deformation of the Central Andes exceeds that in the Southern Andes, as manifest by progressive southward narrowing of the 3 km elevation contour on the map (Fig. 23.1) and by the higher average elevation of the Central Andes. The southward decrease in shortening is accompanied by an increase in crustal thickness to 70 km or more in the Central Andes.

Present shortening rates averaged over last several million years show a similar north-south trend: the Central Andes are currently shortening at rates of 1–1.5 cm yr<sup>-1</sup> (see Oncken et al., Chap. 1 of this volume, and discussion within), while in the Southern Andes the rates are so low (< 0.5 cm yr<sup>-1</sup>) as to be difficult to estimate (Kley and Monaldi 1998). Several workers attribute this variation in shortening and shortening rates to along-strike differences in the degree of coupling between the Nazca and South American Plates (Lamb and Davis 2003; Yanez and Cembrano 2004; Sobolev et al., Chap. 25 of this volume; Hoffmann-Rothe et al., Chap. 6 of this volume), possibly induced by latitudinal, climate-induced variations in erosion rates and the mechanical properties of the trench fill as well as the age and strength of the oceanic plate.

To better understand these first-order deformational features of the Andes, we developed and applied a new numerical model that incorporates some of the salient, physical features of subduction orogenesis. We employ a backward-modeling approach; i.e., we incorporate data on the recent kinematic, gravitational and thermal states of the South America–Nazca Plate boundary system together with knowledge of the current bathymetry, topography and rheology from geophysical studies to back-calculate the local rates of shortening, thickening and rotation in the upper plate.

These calculations are mechanism-specific; they combine lateral shortening, topography and channel flow. The values obtained for primary orogenic features (e.g., orogenic geometry in map view, lithospheric thickness, rota-

tion rates) are then compared with the available data on current rates of shortening (from geological estimations) and rotation (from paleomagnetic studies) to gain insight into the driving mechanisms and parameters controlling Andean orogenesis. Therefore, the criterion for judging the relative importance of different mechanisms is the degree to which predicted, back-calculated values match current, measured values.

We emphasize that our model is not intended to simulate Andean orogenesis or even to provide a detailed picture of Andean orogenic evolution. Rather, it is a vehicle for conducting a series of experiments and parameter studies, each of which is designed to test the plausibility of various mechanisms proposed for the first-order Andean features described above. From a methodological standpoint, our approach is similar to that adopted by Lithgow-Bertelloni and Gynn (2001) to predict stress field variations over the entire Earth. However, our model deals with a much smaller region and is tailored to account for the specific characteristics of recent Andean subduction orogenesis. The numerical basis of our model (thin viscous sheet approximation), of course, limits our analysis precluding analysis of faulting and thrusting processes.

In the next section, we present details of our mechanical model, including the rheologies of the oceanic lower plate, the continental upper plate and the interplate subduction channel, as well as the way in which we have adapted the thin-sheet approach to examine the proposed orogenic processes. We then present a basic model relevant to Andean orogenesis and analyze how changing model parameters affect Andean deformation, particularly deformation related to the formation of the Bolivian orocline and the Andean Plateau.

### 23.2 Thin-Sheet Approximation Applied to Nazca-South American Subduction Orogenesis

The thin-sheet approximation of England and McKenzie (1982) involved determining the balance of stresses in continental lithosphere subjected to tectonic forces exerted by an undeformable, indenting plate (in their case, Asia and India, respectively). The continental lithosphere was assumed to be a uniform sheet that is not subjected to any basal traction, and whose width and breadth far exceed its thickness. England and McKenzie (1982) suggested that the strain rate of the continental lithosphere does not vary vertically, and that a balance of vertically integrated stresses can approximate the balance of stresses in the lithosphere. Thus, simple 2D equations can be used to approximate the 3D deformation of the continental lithosphere. To apply this general approach to the Nazca-South American subduction orogeny, we have had to make some modifications, as outlined below.

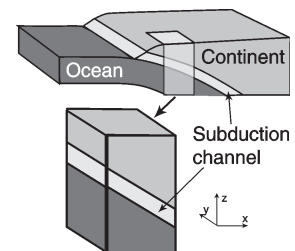
Firstly, we consider the deformation of two plates (Nazca and South America) rather than of just a single indented plate, as in England and McKenzie's (1982) original approach. The Nazca and South American Plates have different characteristics and deformational states: Whereas the western part of the South American continent comprises the Andes and is highly deformed, the Nazca Plate is oceanic and virtually undeformed (Fig. 23.1). The lower plate is, therefore, inferred to be stronger than the upper continental plate.

Subduction of the Nazca Plate beneath South America precludes direct application of the thin-sheet approximation in its classical formulation because the lower plate imposes a basal traction on the overlying continental lithosphere in the vicinity of the subduction zone. This poses a problem because simply introducing additional force into the thin-sheet force balance (e.g., Husson and Ricard 2004) is not compatible with the principle assumption of no basal traction in the thin-sheet approximation (England and McKenzie 1982). We therefore treat the plates' interface as a separate mechanical entity, our so-called "subduction zone", which comprises a thin channel of un- or partly consolidated sediments and their metamorphosed equivalents sandwiched between adjacent parts of the upper and lower plates (Fig. 23.2).

The rocks within this channel, known as the subduction channel (Peacock 1987; Cloos and Shreve 1988a,b; Hoffmann-Rothe et al., Chap. 6 of this volume), are intrinsically weak, the more so if they are subjected to high pore-fluid pressure, as is reasonably expected for subducting oceanic sediments undergoing prograde metamorphic dehydration (e.g., Hacker et al. 2003). These weakening agents are inferred to reduce overall coupling between the upper and lower plates. Thus, the vertically integrated strength of the subduction zone is not only a function of the strengths of the oceanic and continental plates, but also of the dip and strength of the subduction channel. In the Andean case, the subduction channel is assumed to have the same inclination as that of the oceanic slab, dipping 15–30° to the east within the 20–50 km depth interval. This depth interval coincides with the depth interval of seismic coupling (Isacks 1988; Hoffmann-Rothe et al., Chap. 6 of this volume).

For the general purposes of our model, the upper, South American Plate is assumed to comprise a weak Andean orogenic belt and a stronger orogenic foreland. In mak-

**Fig. 23.2.** Subduction zone (*above*) and subduction zone element (*below*) described in the text. See Appendix 23.B for integrated rheology of the subduction zone element



ing this simple assumption, we purposefully ignore evidence that the South American Plate is more complex, with at least two foreland domains (Brazilian shield and basement arches of the Sierras Pampeanas; Kley et al. 1999; Sobolev et al., Chap. 25 of this volume) and with variations in thickness and thermal properties along the strike of the Andes (e.g., differences between Altiplano and Puna lithospheres, Whitman et al. 1992; Kay et al. 1994). Significant though these differences may seem, they turn out to be small in comparison to the truly large differences between the Andean chain and its foreland.

The assumption that the Andean lithosphere is weaker than its foreland lithosphere is based on several studies indicating that the lithosphere under high-elevated

Andes is thinner (e.g., Whitman et al. 1992; Kay et al. 1994) and hotter (Henry and Pollack 1988; Springer and Förster 1998; Springer 1999) than the lithosphere under undeformed parts of South America (east from Andes). This is especially true for the Puna part of the plateau. The modest deformation of the Andean foreland (east from the orogenic chain, Fig. 23.1) is also a qualitative indication that it is stronger than the orogenic lithosphere.

The existence of weak, mid to lower crust is another property of the Andes that cannot be modeled with the classical thin-sheet approximation. England and McKenzie's (1982) formulation assumes uniform deformation throughout the continental lithosphere. However, this

**Table 23.1.** Parameters of the model

Variable	Description	Value in reference model
$g$	Acceleration due to gravity	$9.8 \text{ m c}^{-2}$
$\rho_m$	Density of mantle lithosphere	$3.3 \times 10^3 \text{ kg m}^{-3}$
$\Phi$	Isostatic amplification factor	$1 - \rho / \rho_m$
<b>Oceanic plate</b>		
$\mu_o$	Characteristic viscosity of lithosphere	$2 \times 10^{24} \text{ Pa s}$
$L_o$	Characteristic thickness of lithosphere	50 km
$\rho$	Density of oceanic crust	$3 \times 10^3 \text{ kg m}^{-3}$
<b>Subduction zone</b>		
$\mu_{xx}$	Viscosity of the subduction zone in the X-direction (east-west)	$3 \times 10^{20} \text{ Pa s}$
$\mu_{yy}$	Viscosity of the subduction zone in the Y-direction (north-south)	$7 \times 10^{22} \text{ Pa s}$
$\mu_{xy}$	Viscosity of the subduction zone in a simple shear	$10^{19} \text{ Pa s}$
$L_s$	Characteristic thickness of the lithosphere in the vicinity of the subduction zone	100 km
<b>Continental plate</b>		
$\mu_{c0}$	Characteristic viscosity of undeformed foreland lithosphere	$7 \times 10^{22} \text{ Pa s}$
$\mu_{c1}$	Characteristic viscosity of orogenic lithosphere	$2.8 \times 10^{21} \text{ Pa s}$
$L_c$	Characteristic thickness of lithosphere	100 km
$\rho$	Density of crust	$2.8 \times 10^3 \text{ kg m}^{-3}$
$H_0$	Thickness of undeformed crust	39 km
$H^*$	Critical thickness of crust for channel flow	62 km
<b>Mid to lower crustal channel</b>		
$h$	Thickness of the channel	10 km
$\mu_{ch}$	Viscosity of the channel rock (changes at critical thickness of the crust, $H^*$ )	$10^{20}/10^{22} \text{ Pa s}$
<b>Characteristic ratios of the model</b>		
$\bar{\mu}_{c1} / \bar{\mu}_{c0}$	Strength of the orogenic lithosphere relative to the strength of the foreland lithosphere	0.04
$\bar{\mu}_{xx} / \bar{\mu}_{c1}$	Strength of the subduction zone relative to the strength of the orogenic Andean lithosphere	0.11
$R_{c/s}$	Relative strength of the subduction zone at $19^\circ \text{ S}$ and at $32^\circ \text{ S}$	1

is unreasonable for the Andes in light of abundant seismic (Swenson et al. 2000; Yuan et al. 2000; Haberland and Rietbrock 2001) and magnetotelluric (Brasse 2002; Haberland et al. 2003) evidence for partial melting (Babeyko et al. 2002; Zandt et al. 2003) in the lower crust beneath the plateau regions. Experimental studies indicate that even minute (= 0.1 vol.%) amounts of partial melt can reduce rock strength by several orders of magnitude (Rosenberg and Handy 2005). Therefore, the partially molten, lower Andean crust is reasonably assumed to be highly mobile, resulting in channel flow (Husson and Sempere 2003; Yang et al. 2003; Gerbault et al. 2005) and non-uniform deformation of the Andean lithosphere.

The parameters listed in Table 23.1 reflect these Andean characteristics and account for the following basic observations mentioned in the introduction:

1. A shortening rate for the Central Andes of 1–1.75 cm yr<sup>-1</sup> and for the Southern Andes of 0–0.5 cm yr<sup>-1</sup>; this corresponds to a difference in shortening rates between center and south of at least 0.9 cm yr<sup>-1</sup>.
2. Ongoing oroclinal bending of the Andes.
3. Orogen-normal, eastward growth of the Andean Plateau in the absence of increasing altitude.

The plate motion rates in Fig. 23.1 are with respect to the mid-Atlantic Ridge (Silver et al. 1998). If we assume that the undeformed Andean foreland is moving westwards at a rate of 3 cm yr<sup>-1</sup>, then shortening of the Andes accommodates only part of this plate motion, while the other part is taken up by the westward motion of the western margin of the South American continent. Because shortening rates decrease from the central to southern parts of the orogen, the motion of the western boundary of South America must decrease accordingly. The slower westward advancement of the Central Andes results in bending of the plate boundary and development of the Bolivian orocline. Thus, our model automatically fulfills condition 2 if condition 1 is satisfied. The mechanism of bending described above is similar to that proposed by Isaacks (1988).

### 23.3 Model Characteristics

We modified the classical thin-sheet approximation of England and McKenzie (1982) by using the higher order, asymptotic analysis of Medvedev and Podladchikov (1999 a, b). Our analysis shows that although the balance of forces presented in England and McKenzie (1982) are applicable to our problem, the kinematic model must be modified to account for mid to lower crustal flow beneath the Andean Plateau (Appendix 23.A; England and McKenzie 1982; Medvedev and Podladchikov 1999a). This results in

the following equations that relate force balance to the thickness and density of the lithosphere:

$$2 \frac{\partial \bar{\tau}_{xx}}{\partial x} + \frac{\partial \bar{\tau}_{yy}}{\partial x} + \frac{\partial \bar{\tau}_{xy}}{\partial y} = g\Phi \rho H \frac{\partial H}{\partial x} \quad (23.1)$$

$$\frac{\partial \bar{\tau}_{xx}}{\partial y} + 2 \frac{\partial \bar{\tau}_{yy}}{\partial y} + \frac{\partial \bar{\tau}_{xy}}{\partial x} = g\Phi \rho H \frac{\partial H}{\partial y}$$

where  $\bar{\tau}$  is a deviatoric stress tensor,  $H$  is the thickness of the crust with density  $\rho$ ,  $\Phi = (1 - \rho/\rho_m)$  is the buoyancy amplification factor, and  $\rho_m$  is the density of the mantle lithosphere. The overbar stands for integration over the depth of the lithosphere. Equation 23.1 assumes no traction at the base of the lithosphere and lithostatic approximation for pressure. The lithosphere is regarded as a viscous fluid, such that the integrated stresses relate to strain rates in the following way:

$$\bar{\tau} = 2\bar{\mu}\dot{\epsilon} \quad (23.2)$$

$$\dot{\epsilon}_{ij} = \frac{\left( \frac{\partial V_i}{\partial x_j} + \frac{\partial V_j}{\partial x_i} \right)}{2}$$

where only the horizontal components of stress and strain rate are considered:  $\{x_p, y_j\} = \{x, y\}$  are the horizontal coordinates, and  $\{V_p, V_j\} = \{V_x, V_y\}$  are the depth-invariant horizontal velocities. In the following subsections, we discuss, in some detail, the parameters of the rheological relation in Eq. 23.2, as well as the deformational processes in the system. The model system is divided into three main types of lithosphere: oceanic, continental, and transitional (the subduction zone).

#### 23.3.1 Oceanic Lithosphere

The strength of the oceanic plate depends on its thermal state, which, in turn, is a function of its age (Turcotte and Schubert 1982). Therefore, we adopt the following relation:

$$\bar{\mu}_o = \mu_o L_o \sqrt{\frac{\text{age}}{\text{average\_age}}} \quad (23.3)$$

where  $\mu_o$  is the characteristic viscosity of the oceanic plate and  $L_o$  is the characteristic thickness of the plate. The average age in this equation is calculated from the 26 to 50 Myr age range of the oceanic crust in this area (Fig. 23.1, Müller et al. 1993). This results in age-dependent variations in the strength of the oceanic plate (Eq. 23.3) of up to a factor of two (Table 23.1).

### 23.3.2 Subduction Zone Elements

The subduction zone elements (Fig. 23.2) comprise layers of oceanic and continental lithosphere, and the subduction channel (Peacock 1987; Cloos and Shreve 1988a,b). This composite structure requires a detailed analysis to complete the integrated rheological relation in Eq. 23.2. We therefore consider stresses associated with each component of the strain-rate tensor in Appendix 23.B and show that the rheological relation in Eq. 23.2, as applied to the subduction zone, can be expressed as:

$$\begin{pmatrix} \bar{\tau}_{xx} \\ \bar{\tau}_{yy} \\ \bar{\tau}_{xy} \end{pmatrix} = 2L_s \begin{bmatrix} \mu_{xx} & 0 & 0 \\ 0 & \mu_{yy} & 0 \\ 0 & 0 & \mu_{xy} \end{bmatrix} \cdot \begin{pmatrix} \dot{\epsilon}_{xx} \\ \dot{\epsilon}_{yy} \\ \dot{\epsilon}_{xy} \end{pmatrix} \quad (23.4)$$

where  $L_s$  is the characteristic thickness of the lithosphere in the subduction zone, and  $\mu_{yy}$ ,  $\mu_{xx}$ , and  $\mu_{xy}$  are viscosities of the subduction zone in the directions of consideration. Note that the thin-sheet approximation used in our study relates the stresses integrated over the depth of the lithosphere to the average strain rate of the lithosphere. Thus, Eq. 23.4 considers only horizontal directions, with the  $X$  axis oriented east-west and the  $Y$  axis north-south.

Appendix 23.B lists the constituent properties of the subduction zone elements. These properties are based on poorly known parameters (e.g., the thickness and viscosity of the subduction channel). Therefore, Eq. 23.4 uses only the most general constraints in Appendix 23.B regarding the anisotropic stiffness of the subduction zone elements. We assume  $\mu_{yy} > \mu_{xx} > \mu_{xy}$  in our reference model (Table 23.1).

### 23.3.3 Continental Lithosphere

The integrated strength of continental lithosphere strongly depends on the thermal state and thickness of the lithosphere (England and McKenzie 1982; Ranalli 1995). However, data on the Earth's thermal field is sparse and South America is no exception. We have, therefore, tried to find some empirical dependence for the strength of the lithosphere on a temperature-dependent parameter that can be easily extracted from available data sets.

To understand variations in the strength of the continental lithosphere, we compared the integrated strength of the lithosphere before and after deformation (Fig. 23.3a). Sudden, uniform thickening of the lithosphere (Fig. 23.3b, dashed line) results in thickening of the strong crustal and upper-mantle layers and, therefore, in a significant in-

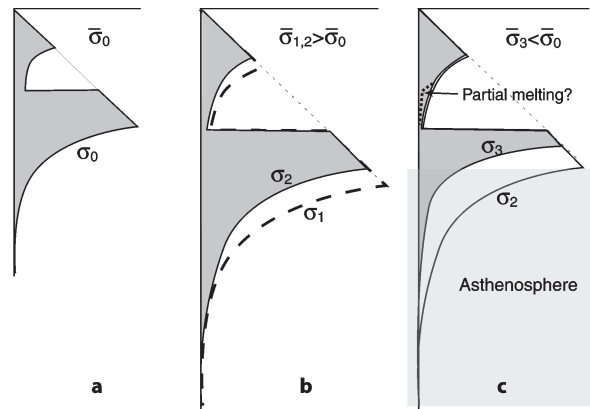


**Fig. 23.3.** Schematic diagram illustrating inferred changes in the strength envelope of the continental lithosphere during orogenesis: **a** Initial strength of the lithosphere  $\bar{\sigma}_0$ ; **b** strength  $\bar{\sigma}_1$  after sudden thickening of the lithosphere (dashed line). Thermal relaxation weakens the lithosphere to  $\bar{\sigma}_2$  (solid line); **c** strength  $\bar{\sigma}_3$  after weakening due to heat advected from the asthenosphere. Note that partial melting in the lower crust does not significantly decrease the integrated strength of the lithosphere

crease of integrated strength. Integrated strength of the lithosphere increases less significant if thickening is gradual. Thermal relaxation and radioactive heating increase average temperature of the lithosphere and make it weaker (Fig. 23.3b, solid line). Applied to Andes, however, this mechanism is proved to be insignificant (model 1 of Babeyko et al. 2002).

Geophysical evidence for detachment of the lithospheric mantle beneath parts of the Andean Plateau (e.g., Yuan et al. 2000) lends credence to the idea that lithospheric weakening is triggered by the upwelling of hot, asthenospheric mantle. The weakening associated with this heat advection from below supersedes the initial strengthening associated with lithospheric thickening. Thus, the contraction of the lithosphere can result in its significant weakening (Dewey 1988; Kay et al. 1994; Babeyko et al. 2006, Chap. 24 of this volume; Sobolev et al. 2006, Chap. 25 of this volume).

A reliable measure of the amount of deformation in the lithosphere is the thickness of the crust. Weakening associated with orogenic thickening is assumed to have affected the entire part of South America considered in our study. Despite the fact that the Andean foreland crust is thinner than the Andean orogenic crust ( $H_0 < H^*$ ), it is much stronger and more viscous. Thus, we relate the integrated strength of the continental lithosphere to the thickness of crust with the following empirical relation (Fig. 23.4):

$$\bar{\mu}_c = \begin{cases} \mu_{c0}L_c & (H < H_0) \\ \mu_{c0}L_c \exp[b(H - H_0)^2] & (H_0 < H < H^*) \\ \mu_{c1}L_c & (H > H^*) \end{cases} \quad (23.5)$$

where  $\mu_{c0}$  and  $L_c$  are the characteristic viscosity and thickness of the continental lithosphere, respectively, and the coefficient  $b = \log(\mu_{c1}/\mu_{c0})/(H_0 - H^*)^2$  is chosen to ensure that viscosity varies continuously from  $\mu_{c0}$  to  $\mu_{c1}$  as a function of crustal thickness,  $H$ . Thus, the changes of rheology, in Eq. 23.4, not only represent changes owing to increased heat advection during thickening, but also to the direct effects of thickening of the orogenic lithosphere.

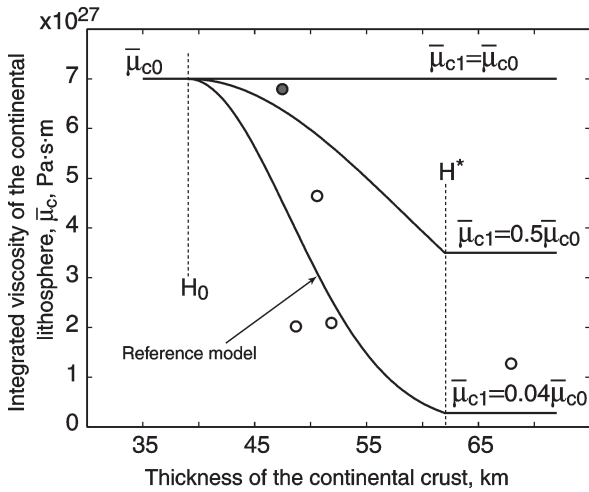


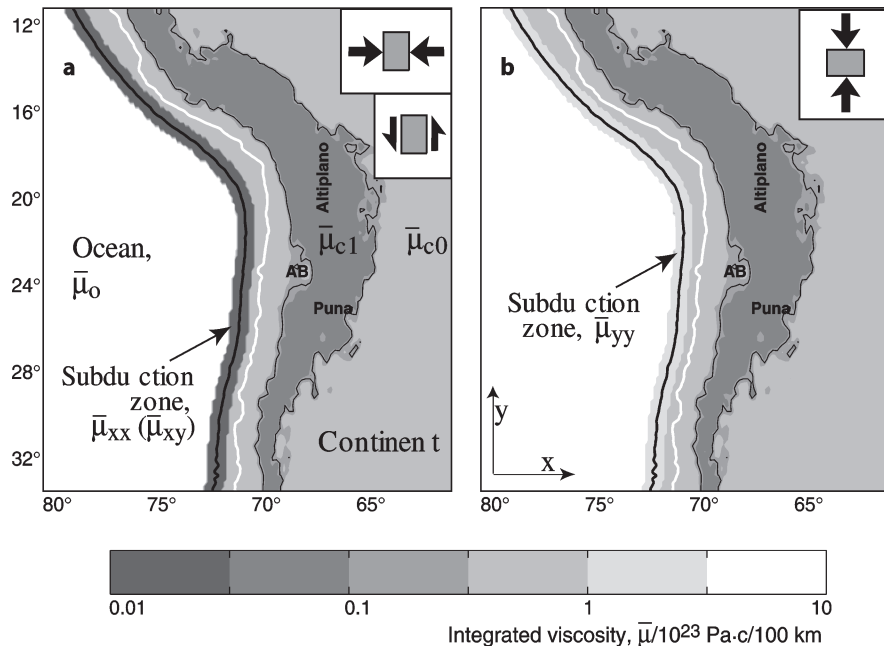
**Fig. 23.4.** Plot of integrated viscosity of the continental lithosphere versus thickness of the continental crust for different ratios (1, 0.5 and 0.04) of the integrated viscosities of the continental foreland ( $\bar{\mu}_{c0}$ ) and orogenic lithosphere ( $\bar{\mu}_{c1}$ ).  $H_0$  and  $H^*$  are the characteristic thicknesses of the crust in the continental foreland and in the orogen, respectively. Circles indicate values obtained from the reference model of Sobolev et al. (Chap. 25 of this volume): *solid circle* = strength of the western margin of the Brazilian shield, *open circles* = strength of the orogenic crust

The thickness of the thickened continental crust,  $H^*$ , is chosen to be 62 km for all the models. This is less than the maximum observed value of 70 km and corresponds to the critical thickness of crust required to drive channel flow, as discussed and estimated in the next section. Thus, the most important rheological parameter of the continental crust is the viscous strength ratio of the orogenic and foreland lithospheres,  $\bar{\mu}_{c1}/\bar{\mu}_{c0} = \mu_{c1}/\mu_{c0}$ . This ratio is 0.04 in the reference model (Fig. 23.4), meaning that the orogenic Andes are 25 times weaker than the Andean foreland. In a separate analysis, we tested different values of this ratio, including situations where the orogenic lithosphere is assumed to be stronger than the foreland ( $\bar{\mu}_{c1}/\bar{\mu}_{c0} > 1$ ).

We note that the viscosity distribution in our model is similar to the integrated effective viscosities in the models of Sobolev et al. (Chap. 25 of this volume; circles and reference model in Fig. 23.4), but that the drop in the integrated viscosity of our reference model is greater than in their model. The 2D models of the Central Andes orogeny in Sobolev et al. (Chap. 25 of this volume) suggest a higher ratio  $\bar{\mu}_{c1}/\bar{\mu}_{c0}$  (0.1) than in our reference model (0.04), as discussed below.

Our model integrates the properties of the continental lithosphere with depth (Fig. 23.5), but, in reality, the strength of the continental lithosphere varies unevenly with depth (Fig. 23.3). Strong layers in the upper crust and lithospheric mantle sandwich a weak, mid to lower crustal layer. Appendix 23.A shows that although the contribution of the weak, lower crustal layer to force balance may be insignificant, this layer contributes significantly to the kinematics of continental deformation.

**Fig. 23.5.** Areal distribution of directional integrated viscosity for different shear configurations in the reference model. **a** Pure shear in an east-west direction or simple shear in a north-south direction; **b** pure shear in a north-south direction. The viscosity of the oceanic plate,  $\bar{\mu}_{c1}$ , is isotropic and depends on the age of the oceanic lithosphere. Likewise, the viscosity of the continental lithosphere,  $\bar{\mu}_c$ , is isotropic but depends strongly on crustal thickness. The strength of the subduction zone is anisotropic (Eq. 23.4). The values of integrated viscosity in this diagram are the integrated viscosity normalized to the viscosity of a characteristic lithosphere (thickness  $L^* = 100$  km, average viscosity  $\mu^* = 10^{23}$  Pa s). Map symbols as in Fig. 23.1



### 23.3.4 Channel Flow and the Orogenic Plateau

We distinguish three types of orogenic processes (Fig. 23.6). The Nazca Plate opposes the westward motion of the South American continent, creating lateral compressional forces,  $F_t$ , that lead to shortening in the Andes (Fig. 23.6b). We term this process “tectonic thickening”. The thickened lithosphere is subjected to a second process, gravity spreading, i.e., deformation of the lithosphere under the force of gravity and buoyancy,  $F_g$  (Fig. 23.6c). Tectonic and gravitational forces,  $F_t$  and  $F_g$ , are the most important forces acting on the lithosphere, as they are responsible for most deformation in the system. Most of thin-sheet approximations applied to model large orogenic systems took into account these two main mechanisms (e.g., England and McKenzie 1982; Yanez and Cembrano 2004), and the Eq. 23.1 in our model balances the integrated stresses caused by these forces.

In Appendix 23.A we consider a third mechanism when analyzing deformation of the continental crust: channel flow in the mid to lower crust (Fig. 23.6d). The importance of channel flow within orogenic continental crust has been

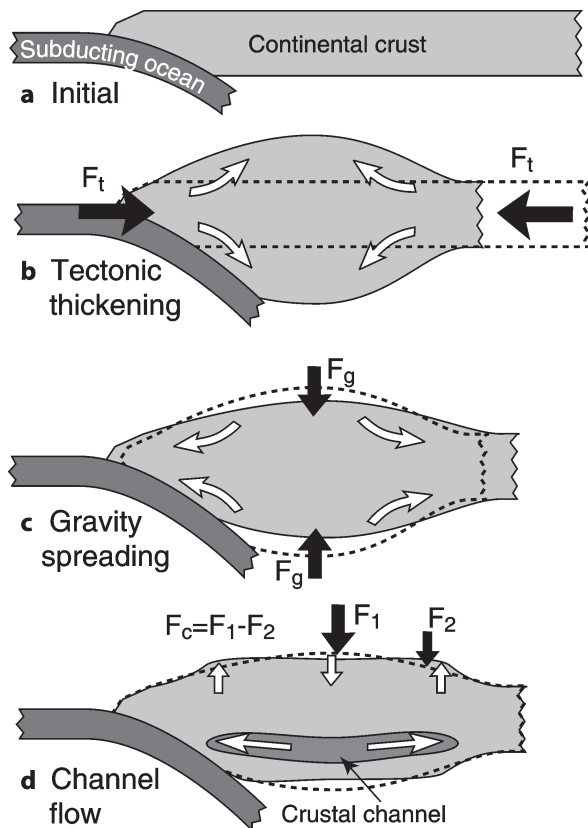


**Fig. 23.6.** Deformation of the upper plate in a subduction orogen. **a** Initial configuration; **b** tectonic thickening; **c** gravity spreading; **d** channel flow creating a plateau. Black arrows illustrate forces acting on the orogenic system, white arrows indicate material flow

discussed extensively in the literature (e.g., Beaumont et al. 2001, 2004; Royden 1996; Clark and Royden 2000; Shen et al. 2001, Gerbault 2005) as being a requisite for development of orogenic plateaus (Royden 1996; Vander-haeghe et al. 2003; Husson and Sempere 2003). The classical thin-sheet approach (England and McKenzie 1982) was developed before channel flow was considered, so that thin-sheet models developed, so far, have not reproduced the topographical features of orogenic plateaus (England and Houseman 1988).

The force  $F_c$  associated with the channel flow is a result of variations of lithostatic loads at the base of thickened continental crust. Differential load of upper crust results in the flow and corresponding drag by the low viscosity channel material on the more competent parts of the lithosphere. This drag is insufficient to contribute to the integrated balance of forces ( $F_c \ll F_g$  and  $F_c \ll F_t$ , Fig. 23.3c, Appendix 23.A), but potential contribution of the channel flow to the kinematics of orogenesis is significant. The following equation describes the evolution of the crustal thickness accounting for both, bulk deformation of the crust and the channel flow (Appendix 23.A):

$$\frac{\partial H}{\partial t} + \left( \frac{\partial V_x H}{\partial x} + \frac{\partial V_y H}{\partial y} \right) - \frac{\rho g h_c^3}{12 \mu_{ch}} \left( \frac{\partial^2 S}{\partial x^2} + \frac{\partial^2 S}{\partial y^2} \right) = 0 \quad (23.6)$$

where  $V_x$  and  $V_y$  are the horizontal velocities obtained from the solution of Eqs. 23.1–23.5. The second bracketed term corresponds to flow in the lower crustal channel and  $S$  is the elevation of topography with respect to sea level (Appendix 23.A, parameters listed in Table 23.1). The influence of the channel increases significantly when the material in the channel becomes very weak during partial melting. Medvedev and Beaumont (in press) show that a decrease of viscosity to  $\mu_{ch} = \mu_p \approx 10^{18} - 10^{20}$  Pa s is sufficient to establish a plateau above the channel. Note, that Eq. 23.6 is used in our model to evaluate the rates of thickness changes ( $\partial H / \partial t$ ), but we do not consider finite-time evolution of the model. Variations of viscosity in the channel are represented in the model by the relation:

$$\mu_{ch} = \begin{cases} \mu_p & (H < H^*) \\ \mu_t & (H > H^*) \end{cases} \quad (23.7)$$

The viscosity in the crustal channel not directly beneath the plateau,  $\mu_t = 10^{22}$  Pa s, was chosen to render the influence of the channel in these regions insignificant. The condition for the transition  $\mu_{ch} = \mu_p \rightarrow \mu_{ch} = \mu_t$  ( $H = H^*$ ) should be consistent with the geometry of the orogen. In particular, the tip of the low-viscosity channel should coincide with the edge of the flat part of the orogen. We term a channel with this configuration a “geometrically consistent channel” (GCC, Fig. 23.7a). If the tip of the channel extends beyond the edge of a plateau, termed an “overdeveloped channel” (OC, Fig. 23.7a), the flux of weak,

partially molten rock is too high to support the overlying plateau, and the plateau collapses. Alternatively, if the channel is too short, an “underdeveloped channel” (UC, Fig. 23.7a), the plateau never becomes flat during shortening, and the margins of the plateau are characterized by high topographic gradients. Of course, the geometry of the Andean orogenic plateau is not as simple as in our experimental model (Fig. 23.7a) and a direct estimation of  $H^*$  is impossible for the Andes.

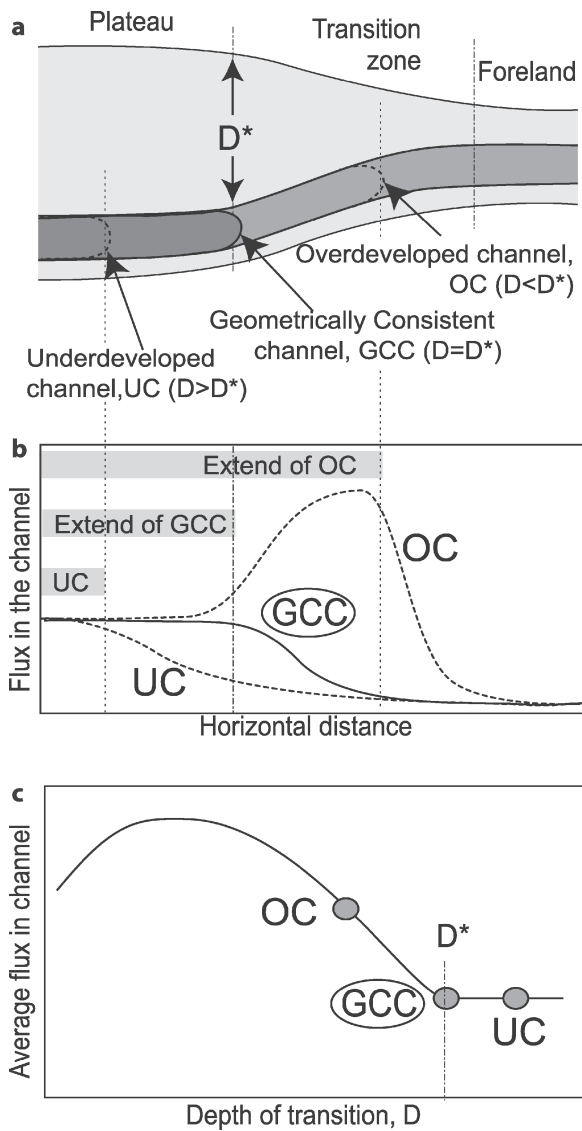


**Fig. 23.7.** General relationship between the lower crustal channel and the orogenic plateau. **a** General view of the plateau margin with different locations for the edge of the low-viscosity channel. *GCC* = channel with its edge directly below the plateau margin at a critical depth,  $D^*$ . *OC* = channel with its edge at a depth less than the critical value needed for sustaining a plateau. *UC* = channel with its edge beneath the plateau. *OC* and *UC* are inconsistent with topography. **b** Variation of flux along the three types of channel. **c** Average flux in the channel versus depth of the channel edge

To specify the condition for a geometrically consistent channel, we consider channel flux for different transitional positions in our experimental model (Fig. 23.7a,b). An estimate of the average flux in the channel for all possible transitions (Fig. 23.7c) shows that the change from a transient to a stable flux occurs where the channel has exactly the same lateral extent as the overlying plateau (point *GCC*, Fig. 23.7c). An absolute value for the flux of low viscosity material in the channel can be calculated for the Central Andes with the following equation (see also Appendix 23.A):

$$|q_c| = \sqrt{q_{cx}^2 + q_{cy}^2} = \frac{\rho g h_c^3}{12\mu_{ch}(H^*)} \sqrt{\left(\frac{\partial S}{\partial x}\right)^2 + \left(\frac{\partial S}{\partial y}\right)^2} \quad (23.8)$$

The absolute value of the flux depends on two parameters: the elevation,  $S$ , and the critical crustal thickness,  $H^*$ . Figure 23.8 presents our calculated average fluxes in low-viscosity channel for different critical thicknesses using actual elevation data from the considered domain of South America (Fig. 23.1). The results in Fig. 23.8 compare well with our analytical predictions (Fig. 23.7) and yield a critical thickness value for Andean crust of  $H^* = 62$  km. This corresponds to a plateau elevation of 3.5 km. We use these parameters in our numerical models.

Equation 23.8 clearly relates the intensity of the channel flow with variations of topography, because the terms in brackets characterize the absolute value of topographic gradient. Results on Fig. 23.8 show that high-elevated Andes (with crustal thickness  $> 57$  km) average topographic gradient decreases with increase of elevation and reaches stable minimal value at 3.5 km elevation ( $H = 62$  km). Thus, the results in Fig. 23.8 indicate that the Andes are typically flatter at elevations exceeding 3.5 km.

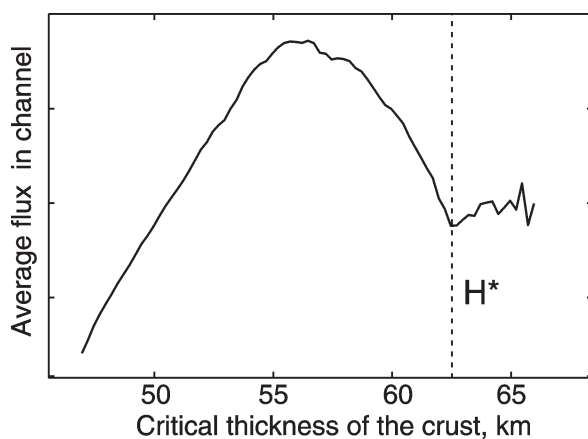


**Fig. 23.8.** Average flux in channels for different values of critical crustal thickness,  $H^*$ . Comparison with Fig. 23.7c indicates that the most suitable value of  $H^*$  is 62 km, corresponding to a plateau elevation of 3.5 km

### 23.3.5 The Numerical Model

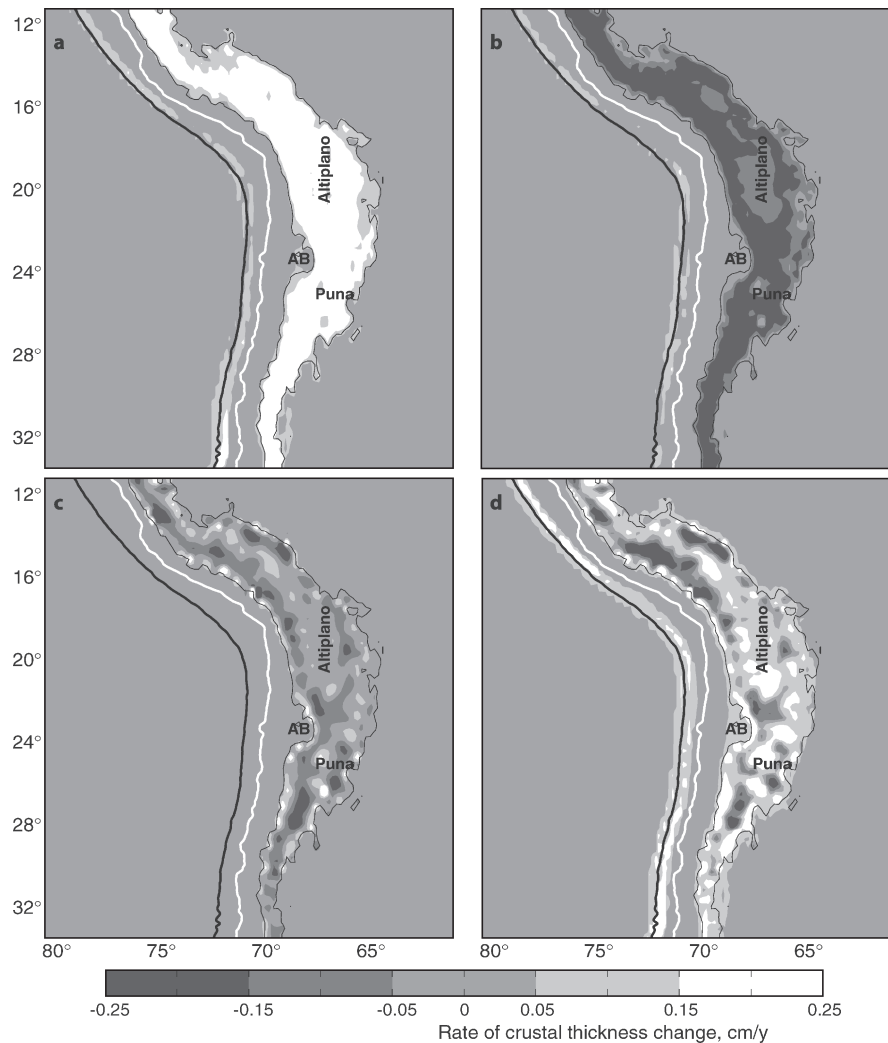
The MATLAB code developed for this study is based on the finite element method (Kwon and Bang 1997). The code uses data regarding the topography and bathymetry (termed  $S$ ), the age of the ocean floor, and the plate boundary from the SFB267 database (<http://userpage.fu-berlin.de/~data/Welcome.html>). Then, the topographic data is converted into crustal thicknesses by using an Airy isostatic model,  $H = H_0 + S/\Phi$  (Turcotte and Schubert 1982). To evaluate unknown initial (undeformed) thickness of the continental crust,  $H_0$ , and isostatic amplification factor,  $\Phi$ , we used estimations of crustal thickness from Götze and Kirchner (1997) and Kirchner et al. (1996). Finally, the code separates the region in question into three parts: oceanic plate, continental plate, and a 100 km wide subduction zone. Table 23.1 lists the parameters of the reference model.

The system of Eqs. 23.1–23.7 was solved using the finite-element approximation based on a second-order in-

terpolation inside the elements. The calculations were performed on a serial PC with a grid of up to  $120 \times 100$  elements (up to  $360 \times 300$  integrating points). The model was designed so that the density of the finite-element grid is a parameter. We used that parameter to test the robustness of the numerical model by comparing results based on the fine and coarse grids.

The boundary conditions for Eq. 23.1 are eastward motion of the Nazca Plate at  $5 \text{ cm yr}^{-1}$  along its western boundary, westward motion of the Brazilian shield at  $3 \text{ cm yr}^{-1}$  along its eastern boundary, and free-slip along the northern and southern boundaries of the model. In the reference model, we ignore the oblique motion of the Nazca Plate by assuming that the northward component of oblique motion can cause local effects along the plate margins, for example, coast-parallel motion and faulting in the South American western fore-arc. We assume, however, that these effects do not significantly affect the general pattern of deformation at the scale of the Andes (Hoffmann-Rothe et al., Chap. 6 of this volume).

**Fig. 23.9.** Rates of thickness change in the reference model due to different modes of orogenic deformation (as in Fig. 23.6). **a** tectonic thickening; **b** gravity spreading; **c** channel flow; **d** all modes simultaneously



## 23.4 Results and Discussion

### 23.4.1 The Reference Model

In this section, we present the results of a reference model that employs the parameters listed in Table 23.1. These parameters were chosen to help us understand the development of primary Andean features, such as the modestly deforming Southern Andes, the bending of the Bolivian orocline, and the development of the Andean Plateau. The model is not designed to match the observations completely. Rather, the goal is to demonstrate that the processes considered above are physically possible given the geodynamic and rheological constraints on Andean orogenesis.

The reference model does not present a unique solution. Analyzing the series of numerical experiments based on different sets of parameters, we chose our reference model (Table 23.1) to illustrate typical results. We discuss variations of parameters in the following sections.

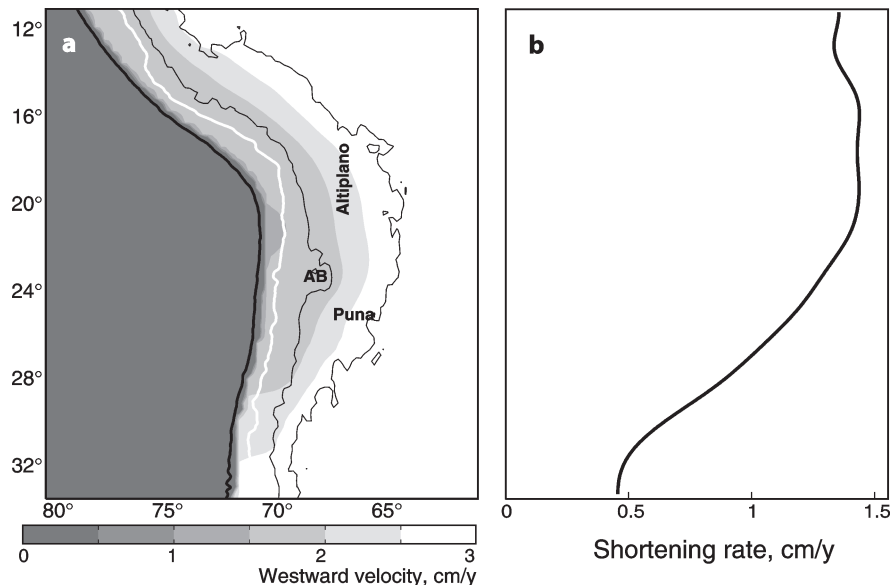
Figure 23.9 illustrates the rates of thickness change, particularly how the three processes considered above (Fig. 23.6) act to change the thickness of the Andean crust. The rate of tectonic thickening (Fig. 23.9a) can be evaluated by eliminating gravity (e.g., by setting the density of the crust to 0 in Eqs. 23.1 and 23.7). As expected, the weaker, orogenic parts of the South American Plate accommodate most of the tectonic thickening in this case. The main factor controlling the rate and distribution of tectonic thickening is the relative integrated strengths of the continental plate, the subduction zone, and the oceanic plate (Fig. 23.5, Table 23.1). Weak orogenic lithosphere, therefore, favors faster, more localized and pronounced thickening in the upper plate, whereas stronger orogenic lithosphere engenders a broader zone of thickening.

The amount and rate of gravitational spreading associated with existing topographic gradients can be evaluated by setting the boundary velocities to 0 (Fig. 23.9d). The main parameter characterizing the rate and distribution of gravity spreading is the strength of the continental plate with respect to the magnitude of the gravity forces acting on the plate surface. Accordingly, a narrow, weak and heavy upper plate favors faster, and more widely distributed, gravitational spreading than a broad, strong, and light upper plate.

The rate of thickness change in the upper plate owing to channel flow was evaluated by setting the bulk velocities in Eq. 23.6 to  $V_x = 0$  and  $V_y = 0$  (in this case the kinematic update, Eq. 23.6, becomes independent from the system Eqs. 23.1–23.5). The influence of the crustal channel is recognizable only in orogenic lithosphere directly beneath the area within 3 km elevation line, where it flattens the topographic relief to a plateau-like morphology. This thickness change rate is heterogeneous, with thinner patches being thickened, and areas of greater thickness becoming somewhat thinner. This smoothing of topography is ascribed to channel flow of partially molten rock. For example, heterogeneous relief of Puna results in uneven distribution rates of thickening, whereas flat topography of the central Altiplano do not result in significant channel flow and in associated thickness changes (cf. Fig. 23.1).

Figure 23.9d presents rates of thickness changes accounting for all three considered mechanisms. The rate of thickening within 3 km elevation line is heterogeneous, tracking the influence of channel flow discussed in the paragraph above. The important feature of the total rate of thickness changes is the active thickening of the crust in the vicinity of the 3 km elevation line. As thickening progresses, the 3 km elevation line expands, tracking the lateral expansion of the Andes. Note, that our numerical model is designed to estimate rates of thickening, not to calculate long-term evolu-

**Fig. 23.10.** Distribution of westward velocity (a) and rate of the horizontal shortening along the Andean chain (b) in the reference model



tion of Andes. Thus, the conclusion about lateral expansion of Andes illustrated by Fig. 23.9d is valid only for the recent state of the Andean orogeny.

Figure 23.10a indicates that the faster westward advancement of the Southern Andes ( $2.5 \text{ cm yr}^{-1}$  from  $30\text{--}35^\circ \text{ S}$ ) than of the Central Andes ( $1\text{--}1.5 \text{ cm yr}^{-1}$  from  $15\text{--}20^\circ \text{ S}$ ) is consistent with the observed bend of the Bolivian orocline. The shortening rate of the Andes in the model (Fig. 23.10b) is equal to the rate at which the foreland approaches the western boundary of the South American Plate. In the model, all of this convergence is accommodated by the deformation of the orogenic lithosphere. The shortening rate varies strongly along strike of the Andean chain, from up to  $1.5 \text{ cm yr}^{-1}$  at  $15\text{--}20^\circ \text{ S}$  (in agreement with Oncken et al., Chap. 1 of this volume) to less than  $0.5 \text{ cm yr}^{-1}$  in the Southern Andes.

### 23.4.2 3D Aspects of the Thin-Sheet Model

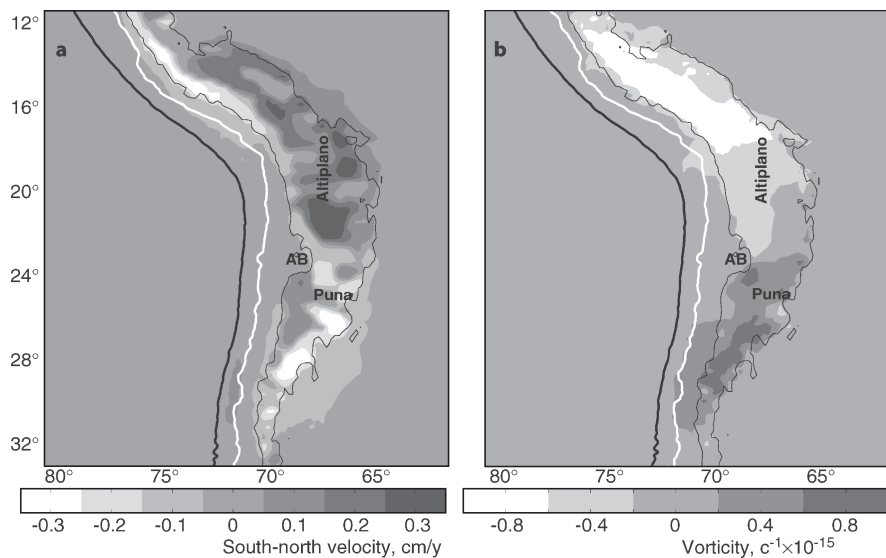
The model used to obtain the results above incorporates an analysis of the horizontal thin sheet with distributed properties, such as integrated viscosity. Similar results within the limits of current accuracy can be obtained by using a series of east-west, cross-sectional models (e.g., Husson and Ricard 2004). The advantage of our model lies in its ability to predict the distribution of some of the 3D features of the Andean orogeny, such as strike-parallel flow of material, and rotations of parts of the Andean crust.

Figure 23.11a depicts the north-south flow of crustal material in the Andes. The flow is presented by an equivalent velocity field for a normalized, 40 km thick crust. Thus, a  $3 \text{ mm yr}^{-1}$  velocity along the southern border of the Puna Plateau represents flow of the normalized, 40 km thick crust at this rate. This significant mass flow must be accounted for when restoring the deformation of the Andes, as already shown by Gerbault et al. (2005).

Figure 23.11b shows a clockwise rotation of the southern part of the Andes and an anti-clockwise rotation of the northern part, consistent with field and paleomagnetic observations (Isacks 1988; Butler et al. 1995; Hindle and Kley 2002; Riller and Oncken 2003; Rousse et al. 2002, 2003). These vorticity values correspond to rotations of  $1.5\text{--}2.2$  degrees per million years, which is comparable to the estimates of Rousse et al. (2003) and Riller and Oncken (2003). The least rotation occurs in the Central Andes between  $20$  and  $24^\circ \text{ S}$ , in agreement with results showing that most rotation in this region occurred earlier, during the Paleogene (Arriagada et al. 2003).

Another 3D aspect of our model is that the properties of the subduction zone can be depth integrated (Appendix 23.B). We performed a sensitivity analysis in order to examine the influence of effective mechanical anisotropy of the subduction elements on Andean-type orogenesis. We did this by varying the viscosity parameters in Eq. 23.5. The reference model (Table 23.1) is based on the relation  $\mu_{yy} \gg \mu_{xx} \gg \mu_{xy}$ . Changing this relationship to  $\mu_{xx} \approx \mu_{xy}$  or  $\mu_{xx} \approx \mu_{yy}$  or  $\mu_{yy} \approx \mu_{xy}$  and tuning rheology to have reasonable results for central and southern parts of our model results in the domination of gravity spreading over tectonic thickening in the Peruvian and Bolivian Andes. This scenario is unrealistic, suggesting that the assumption made in our reference model of subduction zone elements with strongly directional mechanical properties is quite reasonable. This is confirmed by calculations in Appendix 23.B (where it is shown that  $\mu_{yy}$  is of order of  $\mu_c$  or even stronger; and that  $\mu_{xx} \gg \mu_{xy}$ ) and depicted by the ratios in the gray-shaded domains of Figs. 23.12 and 23.13 (for which  $\mu_c \gg \mu_{xx}$ , see next section). Thus, our analytical investigations (Appendix 23.B) and numerical experiments (next chapter) supports the relation of the reference model,  $\mu_{yy} \gg \mu_{xx} \gg \mu_{xy}$ .

**Fig. 23.11.** Distribution of south-north flow in the crust (a, northward flow is positive) and vorticity (b) in the reference model



### 23.4.3 Formation of the Bolivian Orocline and Shortening of the Andes

In this section, we search for parameter values that are consistent with the observed amount and rates of shortening and rotation in the Andes. A series of numerical experiments revealed that the main parameters responsible for oroclinal bending and differential shortening of the Andes are the viscosity ratios  $\bar{\mu}_{c1}/\bar{\mu}_{c0}$  and  $\bar{\mu}_{xx}/\bar{\mu}_{c1}$  (Fig. 23.12). The ratio  $\bar{\mu}_{c1}/\bar{\mu}_{c0}$  (Fig. 23.4) determines the degree to which the orogenic lithosphere weakens as the crust thickens, as well as the degree to which the orogenic lithosphere is weaker than the foreland lithosphere. The ratio  $\bar{\mu}_{xx}/\bar{\mu}_{c1}$  (Fig. 23.5a) is the strength contrast between the orogenic Andean lithosphere and the subduction zone in the direction of subduction. Figure 23.12 depicts the results of 400 numerical experiments conducted to determine which strength ratios are consistent with observed amounts and rates of deformation, all other parameters being held constant at the values listed in Table 23.1. The results show, for example, that the orogenic Andean lithosphere must be at least 14 times weaker than the foreland lithosphere ( $\bar{\mu}_{c1}/\bar{\mu}_{c0} < 0.07$ , Fig. 23.12) for the model to match the observed deformation. Otherwise, the difference in shortening rates between the central and Southern Andes is too low, or the deformation of the Southern Andes is too high.

The calculations used to obtain the results in Fig. 23.12 involve no strike-parallel changes in the rheology of the subduction zone. However, several workers (Yanez and

Cembrano 2004; Lamb and Davis 2003; Sobolev et al., Chap. 25 of this volume; Hoffmann-Rothe et al., Chap. 6 of this volume) emphasize that in the Central Andes the coupling between the upper and lower plates and, therefore, the subduction zone in between are stronger than to the south.

To test the influence of lateral variations in subduction zone rheology, we ran a series of experiments in which the strength of the subduction zone,  $\bar{\mu}_{xx}$ , decreased linearly away from the Central Andes (19° S), both to the north and the south. The measure of this change,  $R_{c/s}$ , is defined as the ratio of  $\bar{\mu}_{xx}$  at 19° S and at 32° S (in the Southern Andes). Figure 23.13 presents results for  $R_{c/s} = 1, 2, \text{ and } 5$ . To fit the observed shortening rates in the Andes, models with  $R_{c/s} > 1$  require less weakening of the orogenic lithosphere (i.e. smaller values for ratio  $\bar{\mu}_{c1}/\bar{\mu}_{c0}$ ) than the reference model with  $R_{c/s} = 1$ . We note that weakening of the orogenic lithosphere, ratio  $\bar{\mu}_{c1}/\bar{\mu}_{c0}$ , in our reference model is several times greater than that predicted by Sobolev et al. (Chap. 25 of this volume), as shown in Fig. 23.4. However, we obtain comparable values of weakening if we use  $R_{c/s} > 1$ , as shown in Fig. 23.13.

Models with an along-strike variation in strength contrast of  $R_{c/s} > 1$  can be considered as a combination of two end-member models. In one (our reference model), the weakening of the Andean orogenic lithosphere compared to the foreland lithosphere is the prime cause of along-strike variations in Andean shortening and oroclinal bending. This model also faithfully reproduces

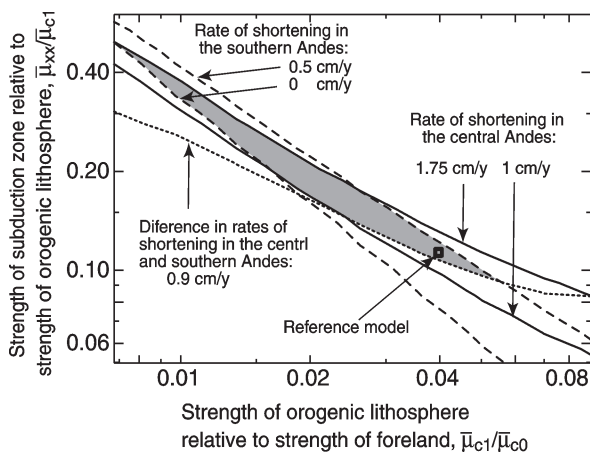


**Fig. 23.12.** Plot of relative strengths showing the range of strength ratios in the model (area shaded gray) that yield deformational rates that are consistent with observed values in the Andes. The lines delimiting this domain represent bounds on the observed shortening rates. *Solid lines:* 1–1.75  $\text{cm yr}^{-1}$  for the Central Andes (18–20° S), *dashed lines:* 0–0.5  $\text{cm yr}^{-1}$  for the Southern Andes (30–32° S), *dotted line:* > 0.9  $\text{cm yr}^{-1}$  for the difference in shortening rates between the central and Southern Andes. *Rectangle* refers to ratios in our reference model

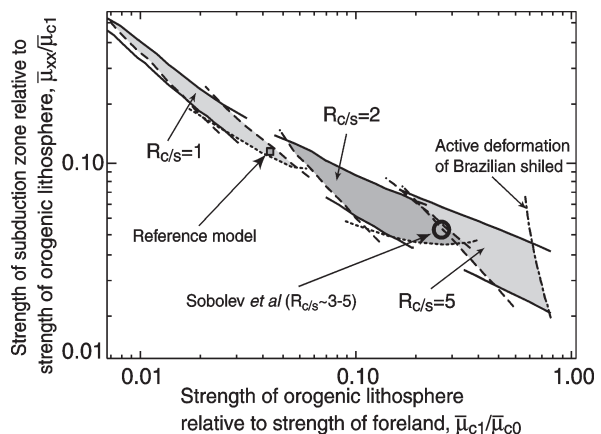


**Fig. 23.13.** Plot of relative strengths with domains of strength ratios (shaded gray) that yield realistic Andean deformational rates for three different values of  $R_{c/s}$  (1, 2 and 5).  $R_{c/s}$  describes the along-strike gradient in the strength of the subduction zone between the Nazca and South American Plates. This strength decreases linearly along strike of the plate margin from  $\bar{\mu}_{xx}$  at 19° S to  $\bar{\mu}_{xx}/R_{c/s}$  at 32° S. The same along-strike gradient is assumed for the subduction zone to the north of 19° S. The lines delimiting the shaded domains are the same as in Fig. 23.12, except that results for  $R_{c/s} = 5$  are limited by the additional constraint that deformation of the Brazilian shield is insignificant. The rectangle refers to ratios in our reference model, the circle refers to ratios in the models of Sobolev et al. (Chap. 25 of this volume)

the observed coincidence of accelerating Andean shortening and decelerating convergence between the Nazca and South American Plates (Hindle et al. 2002) during the most recent 10 Myr. This requires weakening of the orogenic lithosphere by a factor of more than 15, and can only be obtained by assuming unrealistic rheologies or thermal fields. In comparison, the fully numerical cross sectional models in Sobolev et al. (2006, Chap. 25 of this volume) exhibit weakening by no more than a factor of 10.

In the other end-member model, the kinematics of Andean orogenesis are primarily determined by a systematic, along-strike change in the degree of coupling between the Nazca and South American Plates. The importance of that property of the Andean orogeny was outlined in a number of works (Isacks 1988; Lamb and Davis 2003; Yanez and Cembrano 2004; Sobolev et al. 2006, Chap. 25 of this volume). This explains the initiation of oroclinal bending in the absence of orogenic structures along the western side of South America. But without meeting the condition that the orogenic lithosphere is weaker than foreland, the Andes cannot develop any further and the deformation of South America will be well distributed. Figure 23.13 indicates that if  $\bar{\mu}_{c1}/\bar{\mu}_{c0} \sim 1$  or higher, the Brazilian shield will be actively deforming.

Both end-member models have advantages and disadvantages in explaining the salient features of Andean orogenesis, so it is not surprising that reality is best explained by a combination of these end-members. A model in which the strength of the thickened Andean lithosphere decreases by only 5–10 times (Fig. 23.13) and the strength of the subduction zone decreases from the central to the Southern Andes by a factor of 2–5 yields shortening rates that are consistent with observed Recent values.

#### 23.4.4 Comparison with Previous Models

Thickening of the lithosphere yields significant weakening according to Eq. 23.5 (Fig. 23.4). As mentioned above, this weakening is responsible for the formation of the Bolivian orocline and the Andean Plateau, and also explains the modest shortening of the Southern Andes in our reference model. This contrasts with the analog model of Marques and Cobbold (2002), in which the thickened continental lithosphere becomes a strong crustal indenter that effects oroclinal bending. In later stages, this indenter is incorporated into the Andean Plateau. The Andean Plateau develops because the proto-plateau is stronger than the foreland, according to conclusion of Marques and Cobbold (2002) model.

Numerical experiments in which lithospheric strength increases with crustal thickness ( $\bar{\mu}_{c1}/\bar{\mu}_{c0} > 1$ ) exhibit de-

formation of the entire Brazilian shield comparable or even higher than deformation of Andes (Fig. 23.13), which, of course, is entirely unrealistic. The underlying cause of the discrepancy between the results of our reference model (with its requirement that  $\bar{\mu}_{c1}/\bar{\mu}_{c0} < 1$ ) and the Marques and Cobbold (2002) model (2002,  $\bar{\mu}_{c1}/\bar{\mu}_{c0} > 1$ ) is the different conditions at the base of the model: in the analog experiments of Marques and Cobbold (2002), deformation is influenced by the friction along the base of the box, and therefore cannot propagate far from the indenter. In contrast, the base of our numerical model is frictionless (emulating a low-viscosity asthenosphere at the base of the model lithosphere), allowing deformation to propagate far into the upper continental plate, where the weak orogenic lithosphere accommodates most of the shortening.

Channel flow of partially molten rock beneath the high Andes is responsible for flattening of the Andean Plateaux. Without this mechanism, the Andes would thicken continuously in the center instead of growing laterally by thickening at the plateau margins (Lamb 2000; Sobolev et al., Chap. 25 of this volume). The model of Liu et al. (2002) and Yang et al. (2003) shows continuous and nearly uniform uplift of the Andes because the impenetrable boundary in that model is set just outside the Andes, precluding any flow exterior to these mountains and, therefore, precluding lateral expansion of the Andes. We should note that the models of Liu et al. (2002) and Yang et al. (2003) demonstrated clearly the importance of low-crustal flow in the formation of flat topography of the Andean Plateaux.

The age-dependent strength of the oceanic plate (Eq. 23.3) does not significantly influence the pattern of deformation in the Andes in our reference model. This is inconsistent with the results of Yanez and Cembrano's (2004) model in which the age of the subducting Nazca Plate was deemed to be one of the major factors responsible for the development of the Bolivian orocline. In assessing this discrepancy, we point out that the oceanic plate plays a very different role in the two models.

In Yanez and Cembrano's (2004) model, the age of the oceanic lithosphere is used only to estimate the degree of coupling between the undeformable, oceanic, lower plate and the deformable, continental, upper plate. The older and colder the oceanic plate, the greater the degree of interplate coupling. In our model, however, the oceanic plate is strong but deformable, and the interaction between the oceanic and continental plates is specified along their contact within the subduction zone. If we were to relate the properties of the subduction zone to the age of the subducting oceanic plate (e.g., by a special value of the parameter  $R_{c/s}$ ), the distribution of deformation in our model would probably also depend on the age of the oceanic plate.

## 23.5 Conclusions

We present a new numerical thin-sheet model to analyze the recent state of deformation in the Andean orogen. Our numerical experiments show that several first-order features of the Central and Southern Andes can be explained by three aspects which we incorporate as novel features of our model: the effective mechanical anisotropy of the subduction zone, the distribution of integrated strength of the upper continental plate, and channeled flow of partially molten rock at the base of the thickened crust within this upper plate.

Special analysis shows that the subduction zone behaves anisotropically depicting the influence of weak subduction channel and corresponding weakness in the direction of subduction. The degree of that weakness measures the coupling between the Nazca and South American Plates. We also assume that the strength of continental lithosphere depends on the thickness of the crust. Thus, our model enabled us to assess the relative importance of interplate coupling and strength of the orogenic lithosphere with respect to the foreland lithosphere. The validity of the models was determined by their ability to reproduce observed, Recent shortening rates across the Andes.

For uniform coupling between the Nazca and South American Plates, realistic shortening rates were obtained only when the orogenic lithosphere was 20–100 times weaker than the foreland lithosphere. For coupling between the plates that varies along strike of the trench (i.e., from north to south), we found that southward reduction of interplate coupling eases the requirement for strong weakening of the orogenic lithosphere of Andes. Thus, models with calculated shortening rates that are consistent with currently measured rates involve a decrease in interplate coupling by a factor of 2 to 5 from the central to the Southern Andes, and a decrease in the strength ratio of Andean orogenic lithosphere to Andean foreland by a factor of only 5 to 10.

The incorporation of a channel of weak, probably partially molten, middle crust in the upper plate of the model subduction orogen reduces topographic relief in the overlying crust and provides a simple mechanism for the development of the Andean Plateau. The weak crust forms a cushion which flattens the orogen and allows the orogenic plateau to grow laterally, as observed in the Andes today. We ascertain that channel flow is active beneath parts of Andes with an altitude greater than 3.5 km.

Numerical experiments allow us to constrain the rheological parameters associated with presently observed variations in shortening and vorticity along the Andean chain. These variations are also reflected in the measured rates of bending of the Bolivian orocline.

## Acknowledgments

Tough, but adequate reviews by S. Sobolev, M. Gerbault, and J. Cembrano improved significantly the early version of manuscript. Help from H.-J. Götze (associate editor), R. Hackney (geophysical data), A. Britt (English and style corrections), and A. Kellner (some illustrations) is appreciated. This work was supported by the Deutsche Forschungsgemeinschaft in the form of the Collaborative Research Centre “Deformation Processes in the Andes” Grant (SFB 267, Project G2).

## References

- Allmendinger RW, Jordan TE, Kay SM, Isacks BL (1997) The evolution of the Altiplano-Puna Plateau of the Central Andes. *Ann Rev Earth Planet Sci* 25:139–174
- Arriagada C, Roperch P, Mpodozis C, Dupont-Nivet G, Cobbold PR, Chauvin A, Cortés J (2003) Paleogene clockwise tectonic rotations in the forearc of Central Andes, Antofagasta region, Northern Chile. *J Geophys Res* 108(B1): doi 10.1029/2001JB001598
- Babeyko AY, Sobolev SV, Trumbull RB, Oncken O, Lavier LL (2002) Numerical models of crustal scale convection and partial melting beneath the Altiplano-Puna Plateau. *Earth Planet Sci Lett* 199:373–388
- Babeyko AY, et al. (2006) In: Oncken O, Chong G, Frank G, Giese P, Götze H-J, Ramos VA, Strecker MR, Wigger P (eds) *The Andes – active subduction orogeny*. *Frontiers in Earth Science Series*, Vol 1, Springer-Verlag, Berlin Heidelberg New York
- Beaumont C, Jamieson RA, Nguyen MH, Lee B (2001) Himalayan tectonics explained by extrusion of a low-viscosity channel coupled to focused surface denudation. *Nature* 414:738–742
- Beaumont C, Jamieson RA, Nguyen MH, Medvedev S (2004) Crustal channel flows: 1. Numerical models with applications to the tectonics of the Himalayan-Tibetan orogen. *J Geophys Res* 109(B06406): doi 10.1029/2003JB002809
- Brasse H, Lezaeta P, Rath V, Schwalenberg K, Soyer W, Haak V (2002) The Bolivian Altiplano conductivity anomaly. *J Geophys Res* 107(B5): doi 10.1029/2001JB000391
- Butler RF, Richards DR, Sempere T, Marshall LG (1995) Paleomagnetic determinations of vertical-axis tectonic rotations from Late Cretaceous and Paleocene strata of Bolivia. *Geology* 23:799–802
- Carey SW (1958) The orocline concept in geotectonics. *Proc Royal Soc Tasmania* 89:255–288,
- Clark MK, Royden LH (2000) Topographic ooze: building the eastern margin of Tibet by lower crustal flow. *Geology* 28:703–706
- Cloos M, Shreve RL (1988a) Subduction-channel model of prism accretion, melange formation, sediment subduction, and subduction erosion at convergent plate margins: 1. Background and description. *Pure Appl Geophys* 128:455–500
- Cloos M, Shreve RL (1988b) Subduction-channel model of prism accretion, melange formation, sediment subduction, and subduction erosion at convergent plate margins: 2. Implications and discussions. *Pure Appl Geophys* 128:501–545
- Dewey JF (1988) Extensional collapse of orogens. *Tectonics* 7(6): 1123–1139
- England PC, Houseman GA (1988) The mechanics of the Tibetan Plateau. *Phil Trans Royal Soc London A* 326:301–320

- England P, McKenzie D (1982) A thin viscous sheet model for continental deformation. *Geophys J R Astr Soc* 70:295–321. [Correction: England P, McKenzie D (1983) Correction to: A thin viscous sheet model for continental deformation *Geophys J R Astr Soc* 73:523–532]
- Gansser A (1973) Facts and theories on the Andes. *J Geol Soc London* 129:93–131
- Gerbault M, Martinod J, Hérail G (2005) Possible orogeny-parallel lower crustal flow and thickening in the Central Andes. *Tectonophysics* 399:59–72
- Giese P, Scheuber E, Schilling FR, Schmitz M, Wigger P (1999) Crustal thickening processes in the Central Andes and the different natures of the Moho-Discontinuity. *J S Am Earth Sci* 12:201–220
- Götze H-J, Kirchner A (1997) Interpretation of gravity and geoid in the Central Andes between 20° and 29° S. *J S Am Earth Sci* 10:179–188
- Haberland C, Rietbrock A (2001) Attenuation tomography in the western central Andes: a detailed insight into the structure of a magmatic arc. *J Geophys Res* 106(B6):11151–11167
- Haberland C, Rietbrock A, Schurr B, Brasse H (2003) Coincident anomalies of seismic attenuation and electrical resistivity beneath the southern Bolivian Altiplano plateau. *Geophys Res Lett* 30(18): doi 10.1029/2003GL017492,2003
- Hacker BR, Peacock SM, Abers GA, Holloway SD (2003) Subduction factory 2. Are intermediate-depth earthquakes in subducting slabs linked to metamorphic dehydration reactions? *J Geophys Res* 108(B1): doi 10.1029/2001JB001129
- Henry SG, Pollack HN (1988) Terrestrial heat flow above the Andean subduction zone, Bolivia and Peru. *J Geophys Res* 93:15153–15162
- Hindle D, Kley J (2002) Displacements, strains and rotations in the Central Andean Plate boundary. In: Stein S, Freymüller J (eds) Plate boundary zones. AGU Geodynamic Series 30, pp 135–144
- Hindle D, Kley J, Klosko E, Stein S, Dixon T, Norabuena E (2002) Consistency of geologic and geodetic displacements in Andean orogenesis. *Geophys Res Lett* 29: doi 10.1029/2001GL013757
- Hoffmann-Rothe, et al. (2006) In: Oncken O, Chong G, Frank G, Giese P, Götze H-J, Ramos VA, Strecker MR, Wigger P (eds) The Andes – active subduction orogeny. *Frontiers in Earth Science Series, Vol 1*, Springer-Verlag, Berlin Heidelberg New York
- Husson L, Ricard Y (2004) Stress balance above subduction: application to the Andes. *Earth Planet Sci Lett* 222:1037–1050
- Husson L, Sempere T (2003) Thickening the Altiplano crust by gravity-driven crustal channel flow. *Geophys Res Lett* 30: doi 10.1029/2002GL016877
- Isacks BL (1988) Uplift of the Central Andean plateau and bending of the Bolivian Orocline. *J Geophys Res* 93:3211–3231
- James DE (1971) Andean crust and upper mantle structure. *J Geophys Res* 76:3246–3271
- Kay SM, Coira B, Viramonte J (1994) Young mafic back arc volcanic rocks as indicators of continental lithospheric delamination beneath the Argentine Puna plateau, Central Andes. *J Geophys Res* 99(B12):24323–24339
- Kirchner A, Götze H-J, Schmitz M (1996) 3D-density modelling with seismic constraints in the Central Andes. *Phys Chem Earth* 21:289–293
- Kley J, Monaldi CR (1998) Tectonic shortening and crustal thickening in the Central Andes: how good is the correlation? *Geology* 26(8):723–726
- Kley J, Monaldi CR, Salfity JA (1999) Along-strike segmentation of the Andean foreland: causes and consequences. *Tectonophysics* 301:75–94
- Kwon YW, Bang H (1997) The finite element method using MATLAB. CRC Press, New York
- Lamb S (2000) Active deformation in the Bolivian Andes, South America. *J Geophys Res* 105:25627–25653
- Lamb S, Davis P (2003) Cenozoic climate change as a possible cause for the rise of the Andes. *Nature* 425:792–797
- Lithgow-Bertelloni C, Gynn JH (2004) Origin of the lithospheric stress field. *J Geophys Res* 109(B01408): doi 10.1029/2003JB002467
- Liu M, Yang Y, Stein S, Klosko E (2002) Crustal shortening and extension in the Central Andes: insights from a viscoelastic model. In: Stein S, Freymüller J (eds) Plate boundary zones. AGU Geodynamics Series 30, doi 10.1029/030GD19
- MacFadden B, Anaya F, Swisher C III (1995) Neogene paleomagnetism and oroclinal bending of the Central Andes of Bolivia. *J Geophys Res* 100:8153–8167
- Marques FO, Cobbold PR (2002) Topography as a major factor in the development of arcuate thrust belts: insights from sandbox experiments. *Tectonophysics* 348:247–268
- Medvedev S, Beaumont C (in press) Growth of continental plateaux by channel injection: constraints and thermo-mechanical consistency. *Geol Soc London Spec Pub*
- Medvedev SE, Podladchikov YY (1999a) New extended thin sheet approximation for geodynamic applications – I. Model formulation. *Geophys J Int* 136:567–585
- Medvedev SE, Podladchikov YY (1999b) New extended thin sheet approximation for geodynamic applications – II. 2D examples. *Geophys J Int* 136:586–608
- Müller RD, Roest WR, Royer JY, Gahagan LM, Sclater JG (1992) A digital age map of the ocean floor. *SIO Reference Series* 93–30D
- Oncken O, et al. (2006) In: Oncken O, Chong G, Frank G, Giese P, Götze H-J, Ramos VA, Strecker MR, Wigger P (eds) The Andes – active subduction orogeny. *Frontiers in Earth Science Series, Vol 1*, Springer-Verlag, Berlin Heidelberg New York
- Peacock SM (1987) Thermal effects of metamorphic fluids in subduction zones. *Geology* 15:1057–1060
- Ranalli G (1995) Rheology of the Earth, 2nd Ed. Chapman Hall
- Riller U, Oncken O (2003) Growth of the Central Andean Plateau by tectonic segmentation is controlled by the gradient in crustal shortening. *J Geol* 111:367–384
- Rosenberg CL, Handy MR (2005) Experimental deformation of partially melted granite revisited: implications for the continental crust. *J Metamorph Geol* 23:19–28
- Rousse S, Gilder S, Farber D, McNulty B, Torres V (2002) Paleomagnetic evidence of rapid vertical-axis rotation in the Peruvian Cordillera, ca. 8 Ma. *Geology* 30:75–78
- Rousse S, Gilder S, Farber D, McNulty B, Patriat P, Torres V, Sempere T (2003) Paleomagnetic tracking of mountain building in the Peruvian Andes since 10 Ma. *Tectonics* 22(5): doi 10.1029/2003TC001508
- Royden L (1996) Coupling and decoupling of crust and mantle in convergent orogens: implications for strain partitioning in the crust. *J Geophys Res* 101:17679–17705
- Sheffels BM (1995) Mountain building in the Central Andes: an assessment of the contribution of crustal shortening. *Inter Geol Rev* 37:128–153
- Shen F, Royden LH, Burchfiel BC (2001) Large-scale crustal deformation of the Tibetan Plateau. *J Geophys Res* 106:6793–6816
- Silver PG, Russo RM, Lithgow-Bertelloni C (1998) Coupling of South American and African plate motion and plate deformation. *Science* 279:60–63
- Sobolev, et al. (2006) In: Oncken O, Chong G, Frank G, Giese P, Götze H-J, Ramos VA, Strecker MR, Wigger P (eds) The Andes – active subduction orogeny. *Frontiers in Earth Science Series, Vol 1*, Springer-Verlag, Berlin Heidelberg New York
- Springer M (1999) Interpretation of heat-flow density in the Central Andes. *Tectonophysics* 306:377–395
- Springer M, Förster A (1998) Heatflow density across the Central Andean subduction zone. *Tectonophysics* 291:123–139
- Swenson J, Beck S, Zandt G (2000) Crustal structure of the Altiplano from broadband regional waveform modeling: implications for the composition of thick continental crust. *J Geophys Res* 105(B1):607–621

- Turcotte DL, Schubert G (1982) Geodynamics – applications of continuum physics to geological problems. John Wiley, New York
- Vanderhaeghe O, Medvedev S, Beaumont C, Fullsack P, Jamieson RA (2003) Evolution of orogenic wedges and continental plateaux: insights from crustal thermal-mechanical models overlying subducting mantle lithosphere. *Geophys J Int* 153:27–51
- Whitman D, Isacks BL, Chatelain JL, Chiu JM, Perez A (1992) Attenuation of high-frequency seismic waves beneath the Central Andean plateau. *J Geophys Res* 97(B13):19929–19947
- Wigger P, Schmitz M, Araneda M, Asch G, Baldzuhn S, Giese P, Heinssohn WD, Martinez E, Ricaldi E, Röwer P, Viramonte J (1994) Variation in the crustal structure of the southern Central Andes deduced from seismic refraction investigations. In: Reutter K-J, Scheuber E, Wigger P (eds) *Tectonics of the Southern Central Andes*. Springer-Verlag, Berlin Heidelberg New York, pp 23–48
- Yang Y, Liu M, Stein S (2003) A 3-D geodynamic model of lateral crustal flow during Andean mountain building. *Geophys Res Lett* 30(21): doi 10.1029/2003GL018308
- Yañez G, Cembrano J (2004) Role of viscous plate coupling in the late Tertiary Andean tectonics. *J Geophys Res* 109(B02407)
- Yuan X, Sobolev SV, Kind R, Oncken O, Bock G, Asch G, Schurr B, Graeber F, Rudloff A, Hanka W, Wylegalla K, Tibi R, Haberland C, Rietbrock A, Giese P, Wigger P, Röwer P, Zandt G, Beck S, Wallace T, Pardo M, Comte D (2000) Subduction and collision processes in the Central Andes constrained by converted seismic phases. *Nature* 408:958–961
- Zandt G, Velasco A, Beck S (1994) Composition and thickness of the southern Altiplano crust, Bolivia. *Geology* 22:1003–1006
- Zandt G, Leidig M, Chmielowski J, Baumont D (2003) Seismic detection and characterization of the Altiplano-Puna Magma Body, Central Andes. *Pure Appl Geophys* 160:789–807

### Appendix 23.A Stress and Mass Balance in the Thin Viscous Sheet Approach

In this section we derive the governing equations of the thin viscous sheet and assess the validity of the simplifications related to this approach. Here, we analyze only a specific 2D case, as the general theory of the thin-sheet approximation is presented in Medvedev and Podladchikov (1999a, b). The force balance in terms of stresses is:

$$\frac{\partial \sigma_{zz}}{\partial x} + 2 \frac{\partial \tau_{xx}}{\partial x} + \frac{\partial \tau_{xz}}{\partial z} = 0 \quad (23.A1)$$

$$\frac{\partial \tau_{xz}}{\partial x} + \frac{\partial \sigma_{zz}}{\partial z} = \rho g \quad (23.A2)$$

where  $\sigma$  is the full stress tensor and  $\tau$  is its deviatoric part. We use an equality which results from mass conservation and viscous rheology ( $\tau_{xx} + \tau_{zz} = \mu(\epsilon_{xx} + \epsilon_{zz}) = 0$ , and thus pressure  $p = -\tau_{zz} - \sigma_{zz} = \tau_{xx} - \sigma_{zz}$ ). Integration of Eq. 23.A1 over the depth of the lithosphere yields (Medvedev and Podladchikov 1999a):

$$\frac{\partial \bar{\sigma}_{zz}}{\partial x} + 2 \frac{\partial \bar{\tau}_{xx}}{\partial x} = 0 \quad (23.A3)$$

where we use the condition of zero traction on the top and at the base of the lithosphere. The overbars refer to integration over the thickness of the lithosphere. Double integration of Eq. 23.A2 over the lithospheric depth gives:

$$\bar{\sigma}_{zz} = R_z H + \bar{\rho} g - \int \int \frac{\partial \tau_{xz}}{\partial x} dz dz \quad (23.A4)$$

where  $R_z$  is the pressure at the compensation depth and double overbar stands for double integration. The rheology is:

$$\tau_{xz} = \mu \left( \frac{\partial v_x}{\partial z} + \frac{\partial v_z}{\partial x} \right) \quad (23.A5)$$

and therefore the distribution of the horizontal velocity is:

$$v_x(x, z) = V_x(x) + \int_{-L}^z \left( \frac{\tau_{xz}}{\mu} - \frac{\partial v_z}{\partial x} \right) dz \quad (23.A6)$$

where  $V_x$  is the velocity at the base of the lithosphere,  $z = -L$ , and  $v_z$  is vertical velocity.

Equations 23.A1–23.A6 are exact (not approximated) equations for depth integration in the lithosphere (Medvedev and Podladchikov 1999a). The only simplifying assumption made in that system of equations is that the lithosphere behaves as incompressible viscous fluid.

England and McKenzie (1982) simplified these equations by making two assumptions: (i) they ignored shear stress in Eq. 23.A4,  $\tau_{xz} = 0$ ; and (ii) they ignored velocity variations in Eq. 23.A6 and set  $v_x = V_x$ . After substitution of the shortened Eqs. 23.A4 and 23.A6, the governing Eq. 23.A3 becomes:

$$4 \frac{\partial}{\partial x} \left( \bar{\mu} \frac{\partial V_x}{\partial x} \right) = g \Phi \rho H \frac{\partial H}{\partial x} \quad (23.A7)$$

where  $H$  is the thickness of the crust with density  $\rho$ ,  $\Phi = (1 - \rho/\rho_m)$  is the buoyancy amplification factor, and  $\rho_m$  is the density of the mantle lithosphere.

Simplifications (i) and (ii) in England and McKenzie (1982) are justified for a thin sheet with a nearly even strength distribution and subjected to no friction at the top and bottom boundaries. Oceanic lithosphere fulfills these conditions adequately. However, they are not valid for continental lithosphere characterized by significant strength variations (Fig. 23.3). Whereas the weak part of the mantle lithosphere (bounded at the base by  $\tau_{xz} = 0$ ) should not exert any significant shear stress, the strong variations in strength owing to partial melting in the lower crust can result in finite shear stresses.

There is no way of estimating exactly the influence of this shear stress, so we must make some simplifying assumptions. Here, we ease conditions (i) and (ii) by assuming that the shear stress  $\tau_{xz}$  is small, thus rendering the vertical stress in Eq. 23.A4 close to the lithostatic pressure.

The velocity distribution (Eq. 23.A6) can change in the lower crustal channel, especially if partial melting occurs (Fig. 23.3c). Hence, we assume the total velocity to be:

$$v_x = V_x + v_c \quad (23.A8)$$

where  $v_c$  is the velocity in the lower crustal channel. This velocity has a finite value within the channel and is zero outside of it. Note that this perturbation of velocity in the lower crustal channel does not significantly change the normal stress in Eq. 23.A3, as in the following equation:

$$\bar{\tau}_{xx} = 2\bar{\mu} \frac{\partial V_x}{\partial x} + 2 \int_h \mu_{ch} \frac{\partial v_c}{\partial x} dz \approx 2\bar{\mu} \frac{\partial V_x}{\partial x} \quad (23.A9)$$

This is because  $\mu_{ch}$  is much smaller than the average viscosity of the continental lithosphere. The integral in Eq. 23.A9 is taken over the thickness of the low-viscosity channel in the lower crust,  $h$ . Thus, Eq. 23.A7 describes the stress balance for the lithosphere for conditions that are not as restrictive as in England and McKenzie (1982).

Although the velocity correction in Eq. 23.A8 does not change the balance of integrated stresses in the thin sheet, it is significant enough to change both the balance of masses and the changes in crustal thickness. These changes are described with the equation:

$$\frac{\partial H}{\partial t} + \frac{\partial q_x}{\partial x} = 0; \quad q_x = q_{xv} + q_{xv} \quad (23.A10)$$

where  $q_{xv} = (V_x H)$  is the flux corresponding to the bulk velocity,  $V_x$ , and  $q_{xv}$  is the flux corresponding to the additional flow in the lower crustal channel. We adopted a simplified approach to the estimations of the flux,  $q_{xv}$  (Clark and Royden 2000), in which the channel of constant thickness,  $h_c$  occupies the entire width of the continental crust. The flux is then described by:

$$q_{xv} = -\frac{\rho g h_c^3}{12 \mu_{ch}} \frac{\partial S}{\partial x} \quad (23.A11)$$

where  $S$  is the elevation of the continent. Medvedev and Beaumont (in press) show that the viscosity distribution,  $\mu_c$ , should decrease significantly at the edges of the plateau, such that  $\mu_c = \mu_p$  beneath the plateau. Otherwise,  $\mu_{ch} = \mu_t \gg \mu_p$ , assuming that partial melting in the lower crust is responsible for the development of the plateau. Medvedev and Beaumont (in press) show that orogens with a 10 km thick channel can acquire a plateau-like geometry if  $\mu_p \sim 10^{18} - 10^{20}$  Pa s, and  $\mu_t \geq 25 \mu_p$ . Here we associate that rheological transition with a critical thickness of the crust,  $H^*$ :

$$\mu_{ch} = \begin{cases} \mu_p & (H < H^*) \\ \mu_t & (H > H^*) \end{cases}$$

An appropriate value for  $H^*$  is discussed in the main part of the text. **1D->2D!!!**

We analyzed here the classical thin-sheet approach and show that the 3D analog of Eq. 23.A7 (England and McKenzie 1982) can describe the evolution of the two main parts of our model: the Nazca and South American Plates (see Eqs. 23.A1 and 23.A2). The 3D analog of kinematic update (Eqs. 23.A10 and 23.A11) can be easily obtained by adding  $y$ -related component of flux into Eq. 23.A10:

$$\frac{\partial H}{\partial t} + \frac{\partial q_x}{\partial x} + \frac{\partial q_y}{\partial y} = 0$$

where estimation of  $q_y$  can be obtained the same way as for  $q_x$ , simply replacing subscripts and differentiations from  $x$  to  $y$ . Equation 23.A7 does not apply to the subduction zone and is considered in more detail in the text and in Appendix 23.B.

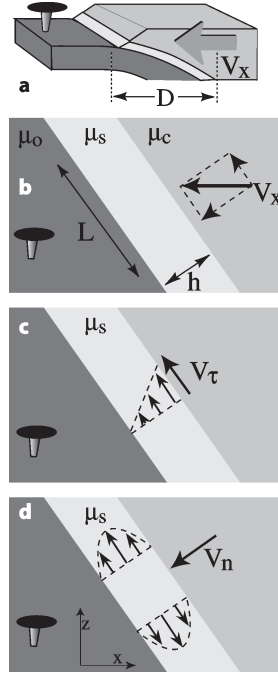
### Appendix 23.B Rheological Properties of the Subduction Zone Elements

The subduction zone elements (Fig. 23.2) include layers of oceanic and continental lithosphere, and the subduction channel. The complicated geometry of the subduction zone requires a detailed analysis of the depth integration. We therefore consider the stresses associated with each component of strain-rate tensor. Even though the subduction zone consists of several elements in the east-west direction (Fig. 23.2), we analyze the entire zone and assume average values for strains and related stresses across it. The following derivations present an approximate analysis aimed mainly at understanding the general characteristics of the thin-sheet representation of the subduction zone. The approximate analysis of this appendix ignores difference between thickness of the subduction zone lithosphere,  $L_s$ , its width,  $D$ , and length of the subduction channel,  $l$ . We understand that these parameters can be different by several times, but we limit our analysis to the qualitative analysis distinguishing only parameters that differ by orders of magnitude. We leave the quantitative estimations of the parameters of the subduction zone to the numerical experiments.

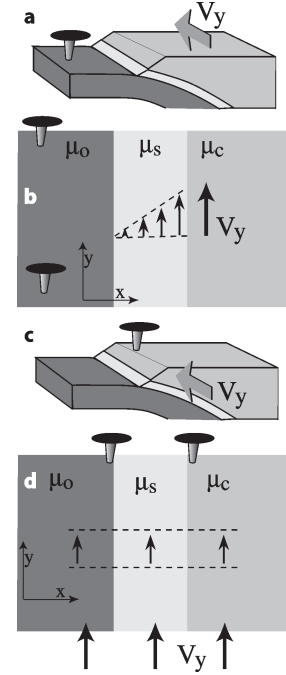
In our analysis, we assume the continental and oceanic crust to be much stronger than the rocks in the subduction channel (Sobolev et al., Chap. 25 of this volume). This assumption allows us to ignore deformation in the continental and oceanic parts of the subduction zone elements, and to concentrate on stresses associated with deformation of the subduction channel only. We also assume that the length of the subduction channel,  $l$ , is greater than its thickness,  $h$ , and introduce the channel aspect ratio,  $\Delta = l/h \gg 1$  (Fig. 23.B1b).

**Fig. 23.B1.**

Estimates of the integrated normal stress due to variations in velocity,  $V_x$ , in the X-direction within the subduction zone. **a** General view; **b** break down of  $V_x$  into velocities parallel and normal to the subduction channel; **c** and **d** flow in the channel at velocity  $v_x$  tangential and normal to the channel boundaries, respectively

**Fig. 23.B2.**

Estimates of the integrated normal stresses in the subduction zone due to variations in velocity,  $V_y$ , in the X-direction (**a** general view, **b** associated flow), and in the Y-direction (**c** general view, **d** associated flow)



Consider stresses associated with variations in the east-west velocity,  $V_x$ , and in the east-west direction,  $X$  (Fig. 23.B1a). Those variations represent the  $xx$  term of the strain-rate tensor,

$$\dot{\epsilon}_{xx} = \frac{\partial V_x}{\partial x} \approx \frac{V_x}{D}$$

( $D$  is the width of the subduction zone). The total variations of velocity can be broken down into two components: channel-parallel and channel-normal,  $V_x = V_\tau + V_n$  (Fig. B1b). The channel-parallel velocity induces Couette flow (Fig. 23.B1c), whereas channel-normal velocity squeezes the channel, inducing Poiseuille flow (Fig. 23.B1d). The average stresses associated with the two components of  $V_x$  are:

$$\sigma_\tau = \frac{\mu_s V_\tau}{h}$$

$$\sigma_n = \frac{2\mu_s V_n l^2}{h^3}$$

where  $\mu_s$  is the viscosity of the rock in the subduction channel. The first equation is a standard expression of the shear stress associated with Couette flow (e.g., Turcotte and Schubert 1982). The second equation represents the average pressure from the channel response on the channel-perpendicular squeezing. Depth-integration yields the shear and normal stresses on the subduction channel:

$$\bar{\sigma}_\tau = \Delta\mu_s V_x$$

$$\bar{\sigma}_n = 2\Delta^3 \mu_s V_x$$

In these expressions, we assume an undeformable continental lithosphere in the presence of the weak subduction channel, rendering  $V_x$  to be invariant with depth. The stress associated with motion parallel to the channel boundaries,  $\sigma_\tau$ , is much smaller than  $\sigma_n$ . Thus, the stress-strain-rate relationship for the  $xx$  component of deviatorial stress can be approximated as:

$$\bar{\tau}_{xx} \approx \bar{\sigma}_n = 2\Delta^3 D \mu_s \dot{\epsilon}_{xx} \quad (23.B1)$$

The shear-stress component,  $\tau_{xy}$ , is reduced to influence of Couette flow in the subduction channel. This is initiated by the difference in the north-south motions across the subduction zone,  $V_y$  (Fig. 23.B2a,b). The shear stress in the channel is therefore:

$$\tau_{xy} = \frac{\mu_s V_y}{h}$$

In this expression we ignore the stresses associated with variations of velocity  $V_x$  in north-south direction,  $\partial V_x / \partial y$ . In the assumptions of our simplified estimations (preferable deformation of the subduction channel) this type of deformation results in rotation of stronger parts and corresponding Couette flow in the channel, which in turn results in stresses of the same order as already estimated. Integration and simplification ( $\dot{\epsilon}_{xy} \approx V_y / D/2$ ) yield the expression:

$$\bar{\tau}_{xy} = 2\Delta D \mu_s \dot{\epsilon}_{xy} \quad (23.B2)$$

The  $yy$  component of the stress tensor is caused by north-south variations in the north-south velocity,  $V_y$  (Fig. 23.B2c,d). The corresponding component of the strain-rate tensor is

$$\dot{\epsilon}_{yy} = \frac{\partial V_y}{\partial y} \approx \frac{V_y}{D_y}$$

where  $D_y$  is the size of the subduction zone element in the  $Y$  direction. The strength of the subduction zone element in this direction is limited by the strength of the competent layers as the deformation cannot be limited to subduction channel only:

$$\tau_{yy} = \frac{2\mu_c V_y}{D_y} \quad (23.B3)$$

$$\bar{\tau}_{yy} = 2\mu_a L_s \dot{\epsilon}_{yy}$$

where  $\mu_a$  is an average viscosity in the subduction zone, and should be limited by values of viscosity of the strong parts of the zone,  $\mu_c$  and  $\mu_o$ . Summarizing Eqs. 23.B1–23.B3, we obtain the following relation for the anisotropic rheology of the subduction zone elements:

$$\begin{pmatrix} \bar{\tau}_{xx} \\ \bar{\tau}_{yy} \\ \bar{\tau}_{xy} \end{pmatrix} = 2 \begin{bmatrix} \Delta^3 D \mu_s & 0 & 0 \\ 0 & L_s \mu_a & 0 \\ 0 & 0 & \Delta D \mu_s \end{bmatrix} \begin{pmatrix} \dot{\epsilon}_{xx} \\ \dot{\epsilon}_{yy} \\ \dot{\epsilon}_{xy} \end{pmatrix} \quad (23.B4)$$

$$\approx 2L_s \begin{bmatrix} \Delta^3 \mu_s & 0 & 0 \\ 0 & \mu_a & 0 \\ 0 & 0 & \Delta \mu_s \end{bmatrix} \begin{pmatrix} \dot{\epsilon}_{xx} \\ \dot{\epsilon}_{yy} \\ \dot{\epsilon}_{xy} \end{pmatrix}$$

The approximate derivations of this section aimed to give the qualitative conclusion that averaged over lithospheric thickness subduction zone behaves anisotropically. Moreover, the parameters of Eq. 23.B4 are difficult to obtain in nature, so we use a simplified version of Eq. 23.B4 (see Eq. 23.4) in our calculations. The analysis presented here, however, can conclude that the viscosity associated with the shear stress component is smaller than one associated with  $\tau_{xx}$ , because  $\Delta \gg 1$ . The above analysis cannot estimate the difference in strength of subduction zone in  $x$  and  $y$  directions, because the components of viscosity in these directions involve  $\Delta \gg 1$  and  $\mu_a \gg \mu_s$  and we leave this analysis to numerical experiments.